공학석사 학위논문

Fault Tolerant Control of Quadrotor based on Barrier Lyapunov Function and Extended State Observer

배리어 르야프노프 함수 및 확장상태 관측기 기반 쿼드로터 고장허용제어

2023 년 2 월

서울대학교 대학원

항공우주공학과

김 미 애

Fault Tolerant Control of Quadrotor based on Barrier Lyapunov Function and Extended State Observer

배리어 르야프노프 함수 및 확장상태 관측기 기반 쿼드로터 고장허용제어

지도교수 김 유 단

이 논문을 공학석사 학위논문으로 제출함

2022 년 12 월

서울대학교 대학원

항공우주공학과

김 미 애

김미애의 공학석사 학위논문을 인준함

2022 년 12 월

위 원 장 김 현 진 (인)

부위원장 김 유 단 (인)

위 원 박 찬 국 (인)

Abstract

Fault Tolerant Control of Quadrotor based on Barrier Lyapunov Function and Extended State Observer

Miae Kim
Department of Mechanical and Aerospace Engineering
The Graduate School
Seoul National University

A fault tolerant control scheme is proposed for a quadrotor under actuator fault with state constraint, model uncertainty, and disturbance using barrier Lyapunov function and nonlinear extended state observer. The proposed control system is divided into two parts: outer loop controller for position tracking and inner loop controller for attitude control. Using the time-varying and time-invariant barrier Lyapunov function, both steady-state and transient performance are guaranteed. To attenuate the effects of uncertainties due to the model uncertainties and disturbances, a nonlinear extended state observer is utilized, which can estimate the total disturbances based on the estimated states of the system. Furthermore, a practical guideline of gain tuning for the proposed control system is proposed considering the analogy of the PID control laws. Numerical simulation is performed to demonstrate the effectiveness of the proposed method.

Keywords: Actuator Fault, Barrier Lyapunov Function, Fault Tolerant Control, Nonlinear Extended State Observer

Student Number: 2021-27861

Contents

List of Tables

List of Figures

Nomenclature

$\alpha_i, i \in \{x, y, z\}$	virtual control function of position tracking controller
$\bar{r}_{1i}, i \in \{\phi, \theta, \psi\}$	modified Euler angle
$\bar{r}_{2i}, i \in \{\phi, \theta, \psi\}$	modified angular rate
$\bar{r}_{3i}, i \in \{\phi, \theta, \psi\}$	total disturbance in angle
$\beta_i, i \in \{\phi, \theta, \psi\}$	virtual control function of attitude controller
$\chi_{1i}, \chi_{2i}, i \in \{\phi, \theta, \psi\}$	state of auxiliary system
δ	design parameter of fal function
$\hat{\bar{r}}_{1i}, \hat{\bar{r}}_{2i}, \hat{\bar{r}}_{3i}, i \in \{\phi, \theta, \psi\}$	estimation of $\bar{r}_{1i}, \bar{r}_{2i}, \bar{r}_{3i}$
$\hat{e}_{1i}, \hat{e}_{2i}, \hat{e}_{3i}, i \in \{x, y, z\}$	estimation of e_{1i}, e_{2i}, e_{3i}
$\lambda_i, i \in \{1, 2, 3, 4\}$	actuator effectiveness factor
$\bar{\mathbf{r}}_\mathbf{d} = [\phi_d, \theta_d, \psi_d]^\intercal$	desired Euler angle
$\mathbf{d_s} = [d_{s\phi}, d_{s\theta}, d_{s\psi}]^\intercal$	system nonlinear term
$\mathbf{d_{p1}}, \mathbf{d_{p2}}, \mathbf{d_{r1}}, \mathbf{d_{r2}}$	unknown function

$\mathbf{p_1} = [x, y, z]^\intercal$	position of the quadrotor with respect to inertial frame
$\mathbf{p_2}$	velocity of the quadrotor with respect to inertial frame
$\mathbf{p_d} = [x_d, y_d, z_d]^\intercal$	desired position
$\mathbf{r_1} = [\phi, \theta, \psi]^\intercal$	Euler angle of the quadrotor with respect to inertial frame
$\mathbf{r_2}$	angular rate of the quadrotor with respect to inertial frame
$\mathbf{u}_\tau = [u_{\tau\phi}, u_{\tau\theta}, u_{\tau\psi}]^\intercal$	control input of attitude controller
$\mathbf{u_p} = [q_x, q_y, q_z]^\intercal$	control input of position tracking controller
$\mathbf{u}$	control input (total thrust of the rotors and the three control torques)
$\mathbf{w_{p1}}, \mathbf{w_{p2}}, \mathbf{w_{r1}}, \mathbf{w_{r2}}$	disturbance
$\Omega_i, i \in \{1, 2, 3, 4\}$	rotor angular speed
$\Omega_{ai}, i \in \{1, 2, 3, 4\}$	actuar rotor angular speed
$\rho_{0i}, \rho_{\infty i}, \rho_{ki}, i \in \{x, y, z\}$	design parameter of rho$_i$
$\rho_{1i}, i \in \{\phi, \theta, \psi\}$	prescribed Euler angle bound
$\rho_{2i}, i \in \{\phi, \theta, \psi\}$	prescribed angular rate bound
$\rho_i, i \in \{x, y, z\}$	prescribed position error bound

θ	design parameter of fal function
$a_i = [a_{1i}, a_{2i}, a_{3i}]$	design parameter of ESO
B	control effectiveness matrix of quadrotor
c_τ	drag moment coefficient
c_f	thrust coefficient
d	distance from the center of mass to the center of each rotor
$e_{1i}, i \in \{x, y, z\}$	modified position error
$e_{2i}, i \in \{x, y, z\}$	modified velocity error
$e_{3i}, i \in \{x, y, z\}$	total disturbance in position
$I = \text{diag}(I_{xx}, I_{yy}, I_{zz})$	inertia matrix of the quadrotor
$k_{1i}, k_{2i}, k_{3i}, i \in \{x, y, z, \phi, \theta, \psi\}$	control gain
$k_{Pi_m}, k_{Di_m}, k_{Ii_m} i \in \{x, y, z, \phi, \theta, \psi\}$	approximated PID gain
$k_{Pi}, k_{Di}, i \in \{x, y, z, \phi, \theta, \psi\}$	approximated PD gain
$l_i, i \in \{x, y, z, \phi, \theta, \psi\}$	ESO gain
m	mass of the quadrotor
$s_{1i}, s_{2i}, i \in \{\phi, \theta, \psi\}$	BLF state transformation of attitude controller
$z_{1i}, z_{2i}, i \in \{x, y, z\}$	BLF state transformation of position tracking controller

g	gravitational acceleration

Chapter 1

Introduction

1.1 Motivation

Recently, unmanned aerial vehicle (UAV) has attracted considerable interest in various fields from industry to military [1]. Among them, quadrotor has been extensively used because of its vertical takeoff and landing, hovering capability, and simple structure [2]. However, quadrotor dynamics may be vulnerable to external disturbances, model uncertainties, and actuator faults due to its strong nonlinearity, and coupling effects resulting from the interaction between aerodynamics, rigid body dynamics, and rotor dynamics [3].

Especially, actuator fault may significantly affect system dynamics [4]. The uncertainties and disturbances can lead to control input saturation and consequently make the system unstable. In this regard, studies on fault tolerant control (FTC) for a quadrotor have been extensively studied to achieve not only high performance but also robustness and reliability. To deal with the problem, many researchers have developed various FTC schemes for quadrotor systems, based on backstepping control [5], sliding mode control [6, 7], feedback linearization [8], and model reference adaptive control [9]. Note that a minor level of uncertainties can be handled by robust control methods. However, maintaining the stability of a quadrotor in case of faults cannot be obtained by solely relying on the robustness of the controller [3].

On the other hand, the disturbance estimation performance of extended state observer (ESO) is closely related to the controller, which influences the performance of the desired controller. That is, poor estimation may yield control inputs that does not properly compensate the disturbances and model uncertainties. If the value of the observer gain is increased to improve the estimation performance, then the possibility of the peaking phenomenon also increases, which leads to the peaking of control inputs and degrading the system performance. Thus, the consideration of selecting ESO parameters, and finding the relations between ESO parameters and control performance are essential for the ESO-based controller.

1.2 Literature Review

An active disturbance rejection control (ADRC) [10] was developed to cope with various kinds of uncertainty, including internal and external disturbances, and time-varying and nonlinear dynamics, and was utilized for FTC design [11,12]. To estimate and compensate for uncertainties and faults, the extended state observer (ESO) can be used as a core part of ADRC, where ESO estimates the model states in that the system states cannot be fully obtained. High-gain linear ESO has been used for the control of nonlinear systems. In the typical high-gain linear ESO, the high-gain parameter is usually powered up to n, which is the dimension of the observed states. The high-gain parameter should be chosen large enough to achieve exact and fast estimation. However, the large value of the high-gain parameter dominates the nonlinear system term, thus could not accurately reflect the system property [13]. Also, high-gain ESO exhibits the peaking phenomenon, which is the phenomenon that the state of the observer showing the peaks of a magnitude when the external environment changes. The high-gain ESO is also known for its sensitivity to high-frequency measurement noise, which makes practical implementation difficult [14]. To cope with this problem, fal-function-based nonlinear ESO was proposed [10, 15, 16]. It was indicated in [17] that fal-function-based nonlinear ESO has a smaller peaking value, faster observation, and better performance under measurement noise than the linear ESO.

Note that state variables are usually subject to various constraints depending on flight conditions and environment. State constraints are usually imposed on the system to guarantee stability [18]. A barrier Lyapunov function (BLF) is utilized to handle the state constraint, which is a kind of control Lyapunov function whose value approaches infinity near certain prescribed bound limits. Owing to the property, BLF-based control guarantees prescribed transient performance, e.g., convergence

rate, steady-state error, and maximum overshoot, by using prescribed time-varying bounds [19]. The time-dependent bound may be set as a monotonically decreasing function of time, and then the transient performance can be specified. A BLF-based FTC methods were proposed for Brunovsky normal form systems using arctangent and logarithmic BLFs [20] and for strict feedback nonlinear systems [21, 22]. In [23], systems with time-varying constraints were considered.

The BLF-based control design is based on the backstepping method. However, the backstepping method itself suffers from the control parameter tuning process due to the repeated differentiation of virtual input commands when dealing with nonlinear systems [24, 25]. To address this issue, formulating a analogy between backstepping control and proportional-integral-derivative (PID) control has been established. For example, PID tuning guideline was proposed based on the backstepping analysis tool in [26]. The backstepping with integral action was proposed in [27], which divides the control law with feedback term and feed-forward terms. Especially, in [28], PID controller was conjugated with BLF to consider the state constraints. However, study on connecting the BLF-based control input to the PID control input has not been done.

1.3 Contributions

In this study, the FTC method based on BLF and ESO is proposed to deal with multiple actuator faults, large disturbances, and model uncertainties. The proposed controller exploits ESO to compensate the uncertainties and faults and utilizes BLF to address the time-varying constraints on position tracking error and the time-invariant constraints on Euler angles and angular rates. Also, this study presents the analogy and relationship between the PID gain structure and the proposed controller, and provides the analysis of ESO parameter selection. The main contributions of this study can be summarized as follows:

1. This study considers general class of nonlinear systems with large uncertainty. With proper state transformation, ESO used in this study can estimate and compensate both matched/mismatched uncertainties and faults.

2. ESO and BLF-based controller are combined to achieve prescribed tracking and transient performance under state constraints and actuator faults. The proposed controller ensures that the position tracking errors, Euler angles, and angular rates are within the prescribed bound.

3. A PID-like control gain is constructed using a BLF-based controller. The analogy and relationship between PID gain and the proposed controller gain are also presented.

4. The effect of ESO parameter is analyzed to the stability and convergence of the system.

1.4 Thesis Overview

The remainder of this thesis is organized as follows. In Chapter 2, problem statement is addressed. Mathematical preliminaries related to BLF are described, and the dynamic models of the quadrotor, the method of system transformation, and the ESO form used in this thesis are introduced. Chapter 3 explains the design process of the proposed FTC control scheme. The proposed FTC scheme consisting of position tracking controller and attitude controller, guarantees the prescribed performance bounds. In Chapter 4, the reformulation of the proposed controller is introduced, which provides the guidelines for gain tuning using the analogy between the proposed FTC scheme and PID control. In Chapter 5, numerical simulations are performed to demonstrate the performance of the proposed FTC scheme. In Chapter 6, concluding remarks and future works are described.

Chapter 2

Problem Statement

2.1 Mathematical Preliminaries

Lemma 2.1. *For any positive constant ρ_i, $i = 1, 2, \ldots, n$, suppose $\mathcal{Z}_i := \{z_i \in \mathbb{R} : -c_{ai} < z_i < c_{bi}\} \subset \mathbb{R}$, $i = 1, 2, \ldots, n$, $\mathcal{N} := \mathbb{R}^l \times \mathcal{Z} \subset \mathbb{R}^{l+1}$ is an open set. Consider the following system.*

$$\dot{\eta} = h(t, \eta) \tag{2.1}$$

where $\eta := [\omega, z] \in \mathcal{N}$, and $h := \mathbb{R}_+ \times \mathcal{N} \to \mathbb{R}^{l+1}$ is piecewise continuous in t and locally Lipschitz in η, and uniformly continuous in t on $\mathbb{R}_+ \times \mathcal{N}$. Suppose that there exist positive definite functions $U : \mathbb{R}^l \times \mathbb{R} \to \mathbb{R}_+$ and $V_i : \mathcal{Z}_i \to \mathbb{R}_+$, $i = 1, 2, \ldots, n$, continuously differentiable in their own domain, such that

$$\begin{aligned} &V_i(z_i) \to \infty \quad as \quad z_i \to -c_{ai} \quad or \quad z_i \to c_{bi} \\ &\gamma_1(||\omega||) \leq U(\omega, t) \leq \gamma_2(||\omega||) \end{aligned} \tag{2.2}$$

where γ_1 and γ_2 are class $\mathcal{K}_\infty$ functions. Let $V(\eta, t) := \sum_{i=1}^{n} V_i(z_i) + U(\omega, t)$, and $z_i(0) \in \mathcal{Z}_i$. If the inequality holds:

$$\dot{V} = \frac{\delta V}{\delta \eta} h + \frac{\delta V}{\delta t} \leq -\gamma V + C \tag{2.3}$$

then $z_i(t)$ remains in the open set $z_i \in (-c_{ai}, c_{bi})$, for $\forall t \in \mathbb{R}_+$.

Proof. This Lemma is the modified version of Lemma 1 in [21] and Lemma 1 in [30] in which autonomous system is considered. Similar process in [21] and [30] is used to prove Lemma 2.1.

The conditions on h ensure the existence and uniqueness of a maximal solution $\eta(t)$ on the time interval $[0, \tau_{max})$, according to [29](p.476, Theorem 54). This implies that $V(\eta(t), t)$ exists for all $t \in [0, \tau_{max})$.

Since $V(\eta(t), t)$ is positive definite and $\dot{V} \leq -\gamma V + C$, $V(\eta(t), t) \leq \left(V(\eta(0), 0) - \frac{C}{\gamma}\right) e^{-\gamma t} + \frac{C}{\gamma} \leq V(\eta(0), 0) + \frac{C}{\gamma}$ for all $t \in [0, \tau_{max})$. From $V(\eta(t), t) := \sum_{i=1}^{n} V_i(z_i) + U(\omega, t)$ and the fact that $V_i(z_i)$ and $U(\omega, t)$ are positive functions, it is clear that $V_i(z_i)$ is also bounded for all $t \in [0, \tau_{max})$. Consequently, from (2.2), $|z_i| \neq -c_{ai}$ and $|z_i| \neq c_{bi}$. Given that $-c_{ai} < z_i(0) < c_{bi}$, it can be inferred that $z_i(t)$ remains in the set $-c_{ai} < z_i < c_{bi}$ for all $t \in [0, \tau_{max})$.

Therefore, there exists a compact subset $\mathbb{K} \subseteq \mathcal{N}$ such that the maximal solution of (2.1) satisfies $\eta(t) \in \mathbb{K}$ for all $t \in [0, \tau_{max})$. As a direct consequence of [29](p.481, Proposition C.3.6), $\eta(t)$ is defined for all $t \in [0, \infty)$, which follows that $z_i(t) \in (-c_{ai}, c_{bi}), \forall t \in [0, \infty)$. □

Lemma 2.2. *([30]) For any positive constant ρ and a scalar x, if $|x| < \rho$, the following inequality holds.*

$$\log\left(\frac{\rho^2}{\rho^2 - x^2}\right) \leq \frac{x^2}{\rho^2 - x^2} \tag{2.4}$$

2.2 Quadrotor Dynamics

The schematic description and the configuration of the frame axes are illustrated in Fig. 2.1.

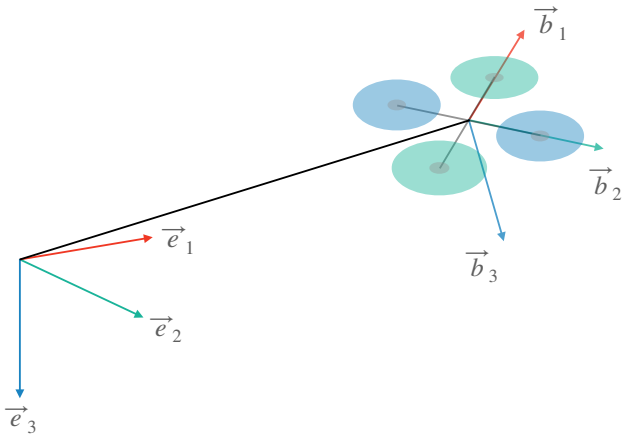

Figure 2.1: Quadrotor model

The translational and rotational dynamic model of the quadrotor with respect to the inertial frame can be represented as follows [32]:

$$
\begin{aligned}
\ddot{x} &= -(c_\phi s_\theta c_\psi + s_\phi s_\psi)\frac{u_1}{m} \\
\ddot{y} &= -(c_\phi s_\theta s_\psi - s_\phi c_\psi)\frac{u_1}{m} \\
\ddot{z} &= g - c_\phi c_\theta \frac{u_1}{m} \\
\ddot{\phi} &= \frac{I_{yy} - I_{zz}}{I_{xx}}\dot{\theta}\dot{\psi} + \frac{d}{I_{xx}}u_2 \\
\ddot{\theta} &= \frac{I_{zz} - I_{xx}}{I_{yy}}\dot{\phi}\dot{\psi} + \frac{d}{I_{yy}}u_3 \\
\ddot{\psi} &= \frac{I_{xx} - I_{yy}}{I_{zz}}\dot{\phi}\dot{\theta} + \frac{1}{I_{zz}}u_4
\end{aligned}
\tag{2.5}
$$

where $c_{(\cdot)}$ and $s_{(\cdot)}$ denote $\cos(\cdot)$ and $\sin(\cdot)$, respectively. The scalar variable m denotes the mass of the quadrotor, g is gravitational acceleration, d is the distance from the

center of mass to the center of each rotor, $I = \text{diag}(I_{xx}, I_{yy}, I_{zz})$ denotes the inertia matrix of the quadrotor, $\mathbf{p_1} = [x, y, z]^\intercal$ and $\mathbf{r_1} = [\phi, \theta, \psi]^\intercal$ represent the position and Euler angle of the quadrotor with respect to the inertial frame, respectively, and $\mathbf{u} = [u_1, u_2, u_3, u_4]^\intercal$ is the control input denoting the total thrust of the rotors and the three control torques, respectively. The relation between the control input $\mathbf{u}$ and the rotor speed can be written as follows [33]:

$$\begin{bmatrix} u_1 \\ u_2 \\ u_3 \\ u_4 \end{bmatrix} = \begin{bmatrix} c_f & c_f & c_f & c_f \\ 0 & -c_f & 0 & c_f \\ c_f & 0 & -c_f & 0 \\ -c_\tau & c_\tau & -c_\tau & c_\tau \end{bmatrix} \begin{bmatrix} \Omega_1^2 \\ \Omega_2^2 \\ \Omega_3^2 \\ \Omega_4^2 \end{bmatrix} \tag{2.6}$$

where Ω_i is the rotor angular speed of the i-th actuator, c_f is the thrust coefficient, and c_τ is the drag moment coefficient. Equation (2.6) can be rewritten as $u = B\Omega^2$, where the matrix B denotes a control effectiveness matrix and $\Omega^2 = [\Omega_1^2, \Omega_2^2, \Omega_3^2, \Omega_4^2]^\intercal$.

In this study, actuator fault representing constant partial loss of effectiveness (LoE) of the rotors is considered. If structural damage in a propeller, such as partial loss of propeller tip, occurs, then a partial loss of thrust is resulted in the corresponding rotor [34]. The actual rotor speed Ω_{ai} can be expressed as $\Omega_{ai} = \sqrt{\lambda_i}\Omega_i$, where $\lambda_i \in [0, 1]$ represents the actuator effectiveness factor: $\lambda_i = 1$ represents a healthy rotor, and $0 \leq \lambda_i < 1$ represents a faulty rotor with a partial LoE.

2.3 System Transformation

2.3.1 Transformation to Normal form SISO System

Consider a following single input single output (SISO) nonlinear system with uncertainties [15].

$$\begin{aligned}
\dot{x}_1(t) &= x_2(t) + h_1(x_1(t), d_1(t)) \\
\dot{x}_2(t) &= x_3(t) + h_2(x_1(t), x_2(t), d_2(t)) \\
&\vdots \\
\dot{x}_{n-1}(t) &= x_n(t) + h_{n-1}(x_1(t), x_2(t), \ldots, x_{n-1}(t), d_{n-1}(t)) \\
\dot{x}_n(t) &= gu(t) + h_n(\mathbf{x}(t), d_n(t)) \\
y(t) &= x_1(t)
\end{aligned} \tag{2.7}$$

where $\mathbf{x}(t) = [x_1(t), x_2(t), \ldots, x_n(t)]^\intercal \in \mathbb{R}^n$ is the state vector, $u(t)$ is the control input, $y(t)$ is the system output, g is constant control effectiveness, d_i, $(i = 1, 2, \ldots, n)$, are the external disturbances, and h_i, $(i = 1, 2, \ldots, n)$ are unknown functions.

Let us define new system variables as

$$\begin{aligned}
\bar{x}_1(t) &= x_1(t) \\
\bar{x}_2(t) &= x_2(t) + h_1(x_1(t), d_1(t)) \\
\bar{x}_3(t) &= x_3(t) + h_2(x_1(t), x_2(t), d_2(t)) + \dot{h}_1(x_1(t), d_1(t)) \\
&\vdots \\
\bar{x}_n(t) &= x_n(t) + \sum_{i=1}^{n-1} h_i^{(n-1-i)}(x_1(t), x_2(t), \ldots, x_i(t), d_i(t))
\end{aligned} \tag{2.8}$$

where $h_i^{(j)}$ denotes the j-th time derivative of h_i. Let the total disturbances of the

system be denoted by

$$\bar{x}_{n+1}(t) = \sum_{i=1}^{n} h_i^{(n-i)}(x_1(t), x_2(t), \ldots, x_i(t), d_i(t)) \tag{2.9}$$

and $\bar{\mathbf{x}}(t) = [\bar{x}_1(t), \bar{x}_2(t), \ldots, \bar{x}_n(t)]^\intercal$. Then, Eq. (2.7) can be rewritten as the following normal form SISO system.

$$\begin{aligned} \dot{\bar{\mathbf{x}}}(t) &= A_n \bar{\mathbf{x}}(t) + B_n[gu(t) + \bar{x}_{n+1}(t)] \\ y(t) &= x_1(t) \end{aligned} \tag{2.10}$$

where

$$A_n = \begin{bmatrix} 0 & I_{(n-1)\times(n-1)} \\ 0 & 0 \end{bmatrix}, \quad B_n = \begin{bmatrix} 0 & 0 & \ldots & 0 & 1 \end{bmatrix}^\intercal$$

2.3.2 Transformation of quadrotor Dynamics

Consider the quadrotor dynamics (2.5) with $\mathbf{w_p}$ and $\mathbf{w_r}$, which represent all the disturbances effecting the quadrotor, such as disturbance, model uncertainty, and fault, and $\mathbf{d_p}(\mathbf{p_1}, \mathbf{p_2}, \mathbf{w_p})$ and $\mathbf{d_r}(\mathbf{r_1}, \mathbf{r_2}, \mathbf{w_r})$ are unknown functions, with nonlinear term of the system $\mathbf{d}_s = [d_{s\phi}, d_{s\theta}, d_{s\psi}]^\intercal$, where $\mathbf{p_1} = [x, y, z]^\intercal$, $\mathbf{r_1} = [\phi, \theta, \psi]^\intercal$. Now, Eq. (2.5) can be represented as

$$\begin{aligned} \dot{\mathbf{p}}_\mathbf{1} &= \mathbf{p_2} \\ \dot{\mathbf{p}}_\mathbf{2} &= \mathbf{u_p} + \mathbf{d_p}(\mathbf{p_1}, \mathbf{p_2}, \mathbf{w_p}) \\ \dot{\mathbf{r}}_\mathbf{1} &= \mathbf{r_2} \\ \dot{\mathbf{r}}_\mathbf{2} &= \mathbf{u}_\tau + \mathbf{d}_s + \mathbf{d_r}(\mathbf{r_1}, \mathbf{r_2}, \mathbf{w_r}) \end{aligned} \tag{2.11}$$

where $\mathbf{u_p} = [q_x, q_y, q_z]^\intercal$, $\mathbf{u}_\tau = [u_{\tau\phi}, u_{\tau\theta}, u_{\tau\psi}]^\intercal$,

$$\begin{aligned} d_{s\phi} &= \frac{I_{yy} - I_{zz}}{I_{xx}} \dot{\theta}\dot{\psi} \\ d_{s\theta} &= \frac{I_{zz} - I_{xx}}{I_{yy}} \dot{\phi}\dot{\psi} \\ d_{s\psi} &= \frac{I_{xx} - I_{yy}}{I_{zz}} \dot{\phi}\dot{\theta} \end{aligned} \tag{2.12}$$

and

$$\begin{aligned} q_x &= -(c_\phi s_\theta c_\psi + s_\phi s_\psi)\frac{u_1}{m} \\ q_y &= -(c_\phi s_\theta s_\psi - s_\phi c_\psi)\frac{u_1}{m} \\ q_z &= g - c_\phi c_\theta \frac{u_1}{m} \\ u_{\tau\phi} &= \frac{d}{I_{xx}} u_2 \\ u_{\tau\theta} &= \frac{d}{I_{yy}} u_3 \\ u_{\tau\psi} &= \frac{1}{I_{zz}} u_4 \end{aligned} \tag{2.13}$$

Assumption 2.1. *For the external disturbances and reference signal, we assume that there exist constants $M_1, M_2 > 0$ such that*

$$\sup_{t\in[0,\infty)} ||\tilde{\mathbf{p}}_\mathbf{d}|| \leq M_1, \quad \sup_{t\in[0,\infty)} ||\tilde{\mathbf{w}}|| \leq M_2 \tag{2.14}$$

where $\tilde{\mathbf{p}}_\mathbf{d} = [\mathbf{p_d}, \dot{\mathbf{p}}_\mathbf{d}]$ and $\tilde{\mathbf{w}} = [\mathbf{w_p}, \mathbf{w_r}, \dot{\mathbf{w}}_\mathbf{p}, \dot{\mathbf{w}}_\mathbf{r}]$

By means of calculation, the actual input u_1 can be obtained as follows:

$$u_1 = m\sqrt{q_x^2 + q_y^2 + (q_z^2 - g)} \tag{2.15}$$

Also, the desired Euler angles ϕ_d and θ_d can be obtained as follows:

$$\begin{aligned} \phi_d &= \arcsin\left(-\frac{m}{u_1}(q_z s(\psi_d) - q_y c(\psi_d))\right) \\ \theta_d &= \arctan\left(\frac{1}{q_z - g}(q_x c(\psi_d) + q_y s(\psi_d))\right) \end{aligned} \tag{2.16}$$

Let us define the position error as $\mathbf{e_1} = [e_{1x}, e_{1y}, e_{1z}]^\intercal = \mathbf{p_1} - \mathbf{p_d}$, $\mathbf{e_2} = [e_{2x}, e_{2y}, e_{2z}]^\intercal = \mathbf{p_2} - \dot{\mathbf{p}}_\mathbf{d} + \mathbf{d_{p1}}$, and let the total disturbances $\mathbf{e_3} = [e_{3x}, e_{3y}, e_{3z}]^\intercal = \dot{\mathbf{d}}_\mathbf{p1} + \mathbf{d_{p2}} - \ddot{\mathbf{p}}_\mathbf{d}$, where $\mathbf{p_d} = [x_d, y_d, z_d]^\intercal$ is the desired position. The position error dynamics of the quadrotor can be transformed into the following normal form subsystem.

$$\begin{aligned} \dot{\mathbf{e}}_\mathbf{1} &= \mathbf{e_2} \\ \dot{\mathbf{e}}_\mathbf{2} &= \mathbf{e_3} + \mathbf{u_p} \end{aligned} \tag{2.17}$$

Similarly, let $\mathbf{r_1} = [r_{1\phi}, r_{1\theta}, r_{1\psi}]^\intercal = [\phi, \theta, \psi]^\intercal$, $\mathbf{r_2} = [r_{2\phi}, r_{2\theta}, r_{2\psi}]^\intercal = [p, q, r]^\intercal$, and define new state variable for total disturbances of rotational dynamics as $\mathbf{r_3} = [r_{3\phi}, r_{3\theta}, r_{3\psi}]^\intercal = \mathbf{d}_s + \mathbf{d_r}$. Then, the rotational dynamics of the quadrotor can be transformed into the following normal form subsystem.

$$\begin{aligned} \dot{\mathbf{r}}_\mathbf{1} &= \mathbf{r_2} \\ \dot{\mathbf{r}}_\mathbf{2} &= \mathbf{r_3} + \mathbf{u}_\tau \end{aligned} \tag{2.18}$$

2.4 Extended State Observer

In order to estimate and compensate total disturbances, ESO is constructed for each SISO subsystem of the modified position error dynamics (2.17), and rotational dynamics (2.18). Throughout this paper, $\hat{(\cdot)}$ represents the estimate of $(\cdot)$. The ESO dynamics can be represented as [16].

$$\begin{aligned}
\dot{\hat{e}}_{1i} &= \hat{e}_{2i} + \frac{a_{1i}}{l_i}\ \mathrm{fal}(l_i^2(e_{1i} - \hat{e}_{1i})) \\
\dot{\hat{e}}_{2i} &= \hat{e}_{3i} + u_{pi} + a_{2i}\ \mathrm{fal}(l_i^2(e_{1i} - \hat{e}_{1i})) \quad , \quad i = x, y, z \\
\dot{\hat{e}}_{3i} &= a_{3i} l_i\ \mathrm{fal}(l_i^2(e_{1i} - \hat{e}_{1i}))
\end{aligned} \tag{2.19}$$

and

$$\begin{aligned}
\dot{\hat{r}}_{1i} &= \hat{r}_{2i} + \frac{a_{1i}}{l_i}\ \mathrm{fal}(l_i^2(r_{1i} - \hat{r}_{1i})) \\
\dot{\hat{r}}_{2i} &= \hat{r}_{3i} + u_{\tau i} + a_{2i}\ \mathrm{fal}(l_i^2(r_{1i} - \hat{r}_{1i})) \quad , \quad i = \phi, \theta, \psi \\
\dot{\hat{r}}_{3i} &= a_{3i} l_i\ \mathrm{fal}(l_i^2(r_{1i} - \hat{r}_{1i}))
\end{aligned} \tag{2.20}$$

where the design parameter, $a_i = [a_{1i}, a_{2i}, a_{3i}]$, are chosen so that the following matrix is Hurwitz [16]:

$$\begin{bmatrix} -a_{1i} & 1 & 0 \\ -a_{2i} & 0 & 1 \\ -a_{3i} & 0 & 0 \end{bmatrix} \tag{2.21}$$

Note that l_i is the tuning parameters according to accuracy requirement and the variation of the total disturbances. The 'fal' function is defined as [10],

$$\mathrm{fal}(x) = \begin{cases} x, & |x| \le \delta \\ |x|^{\theta'} \mathrm{sign}(x), & |x| > \delta \end{cases} \tag{2.22}$$

where $\theta' \in (0,1)$ is constant, which affects the measurement accuracy, and $\delta > 0$ is a design parameter. By using 'fal' function, the designed ESO is less sensitive to the measurement noise for large l_i because the noise is magnified to be $(2\theta'-1, 2\theta', 2\theta'+1)$, less than $(1,2,3)$ of the Linear ESO [16].

Chapter 3

Fault Tolerant Controller Design

The objective of the controller in this study is to design a control input, $\mathbf{u}$, such that the quadrotor, in the presence of internal and external disturbances and actuator faults, can satisfy the following conditions.

1. Position tracking error $\mathbf{e_1}$ remains in the predefined performance bound.
2. Euler angle $\mathbf{r_1}$ and angular rates $\mathbf{r_2}$ remain in the predefined constraint bound.

In this section, the FTC method proposed in this study is explained. The overall configuration of the proposed FTC method is shown in Fig. 3.1.

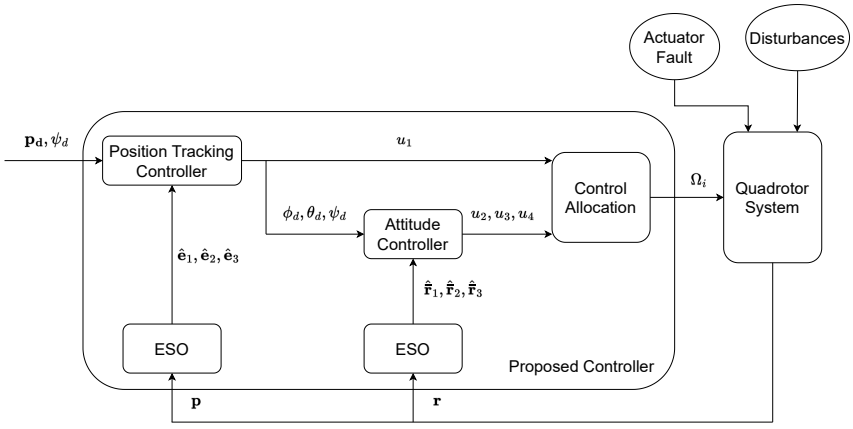

Figure 3.1: Block diagram of the proposed control system

3.1 Position Tracking Controller

The purpose of the position tracking controller is to make the position tracking error $\mathbf{e_1}$ satisfy the following inequality to guarantee the prescribed performance.

$$-\rho_i(t) \leq e_{1i}(t) \leq \rho_i(t), \quad i = x, y, z \tag{3.1}$$

where $\rho_i(t)$ is predefined strictly decreasing, differentiable, and bounded functions, given by $\rho_i(t) = (\rho_{0i} - \rho_{\infty i})e^{-\rho_{k_i} t} + \rho_{\infty i}$, $\lim_{t\to\infty} \rho_i(t) = \rho_{\infty i}$. By selecting the appropriate parameters such as ρ_0, ρ_∞, and ρ_{k_i}, the desired transient performance can be guaranteed. Note that ρ_0 constrains the maximum overshoot, ρ_∞ constrains the steady-state error, and ρ_{k_i} adjusts the convergence rate.

The control design proposed in this study is based on backstepping with symmetric time-varying BLF. Let us define $z_{1i} = e_{1i}/\rho_i$, $z_{2i} = e_{2i} - \alpha_i$, for $i = x, y, z$, where α_i's are virtual control inputs. The controller design process is given as follows [23]:

Step 1: Define the Log-BLF as follows:

$$V_{1i} = \frac{1}{2}\log\left(\frac{\rho_i^2}{\rho_i^2 - e_{1i}^2}\right) = \frac{1}{2}\log\left(\frac{1}{1 - z_{1i}^2}\right) \tag{3.2}$$

It is clear that V_{1i} is positive definite and continuously differentiable in the set $|z_{1i}| < 1$. Differentiating V_{1i} and using Eq. (2.17) yields

$$\dot{V}_{1i} = \frac{z_{1i}}{1 - z_{1i}^2}\frac{1}{\rho_i}(e_{2i} - \dot{\rho}_i z_{1i}) = \frac{z_{1i}}{1 - z_{1i}^2}\frac{1}{\rho_i}(z_{2i} + \alpha_i - \dot{\rho}_i z_{1i}) \tag{3.3}$$

Now, let us define $\alpha_i = \dot{\rho}_i z_{1i} - \rho_i k_{1i} z_{1i}$, with $k_{1i} > 0$. Then, we have $\dot{V}_{1i} = \frac{z_{1i}}{1-z_{1i}^2}\frac{1}{\rho_i}(z_{2i} - \rho_i k_{1i} z_{1i})$.

Step 2: Define the quadratic functions $V_{2i} = z_{2i}^2/2$. Design control input q_i as:

$$q_i = -e_{3i} + \dot{\alpha}_i - k_{2i} z_{2i} - \frac{z_{1i}}{1 - z_{1i}^2} \frac{1}{\rho_i}, \quad k_{2i} > 0 \tag{3.4}$$

Using (2.17), (3.3), (3.4), and Lemma 2.2, the time derivative of $V_i = V_{1i} + V_{2i}$ becomes

$$\begin{aligned} \dot{V}_i &= -k_{1i} \frac{z_{1i}^2}{1 - z_{1i}^2} - k_{2i} z_{2i}^2 \\ &\leq -\gamma_i V_i \end{aligned} \tag{3.5}$$

where $\gamma_i = \min\{2k_{1i}, 2k_{2i}\}$.

Theorem 3.1. *Consider the position error dynamics of the quadrotor (2.17) with control input (3.4) and observer (2.19), and Assumption 2.1. If the initial condition satisfies $|e_{1i}(0)| < \rho_i(0)$, the symmetric time-varying constraint is not violated, i.e., $|e_{1i}(t)| < \rho_i(t)$ for all $t > 0$, and the closed-loop signals z_{1i} and z_{2i} are uniformly bounded.*

Proof. The initial condition requirement is equivalent to $|z_{1i}(0)| < 1$, $\forall t$. Then, Lemma 2.1 ensures that $|z_{1i}(t)| < 1$, which means that $|e_{1i}(t)| < \rho_i(t)$.
Integrating both side of the inequality of Eq. (3.5) yields $V_i(t) \leq V(0)e^{-\gamma_i t}$, $\forall t > 0$, which leads to

$$\frac{1}{2} \log \left(\frac{1}{1 - z_{1i}^2} \right) \leq V_i(0) e^{-\gamma_i t} \tag{3.6}$$

Taking the exponent arithmetic on both sides and reformulating yield:

$$|z_{1i}| \leq \sqrt{1 - e^{-2V_i(0)e^{-\gamma_i t}}} < 1, \quad \forall t > 0 \tag{3.7}$$

Furthermore, since $\frac{1}{2} z_{2i}^2 \leq V_i(0)e^{-\gamma_i t}$, it can be shown that $||z_{2i}|| \leq \sqrt{2V_i(0)e^{-\gamma_i t}}$,

$\forall t > 0.$ $\square$

3.2 Attitude Controller

The purpose of the attitude controller is to make the Euler angles and angular rates satisfy the following inequality to guarantee the prescribed performance.

$$-\rho_{1i} \leq r_{1i} \leq \rho_{1i}, \quad -\rho_{2i} \leq r_{2i} \leq \rho_{2i}, \quad i = \phi, \theta, \psi \tag{3.8}$$

where ρ_{1i} and ρ_{2i} are predefined positive scalars.

When an actuator fault occurs in the system with disturbances, it may lead to input saturation and cause unstable. Considering control effectiveness matrix of quadrotor in Eq. (2.6), the roll and pitch moments, u_2 and u_3, are determined only by the second and fourth rotors and the first and third rotors, respectively. It means that if the fault occurs at rotor 1, the fault will affect pitch moment more than others such as thrust or yaw moment. To compensate the effect of the input saturation, let us introduce an auxiliary system, which considers the difference between the actual control input and the desired control input, i.e., $\triangle u = \text{sat}(u) - u$ [31, 35, 36].

Assumption 3.1. *Consider the situation that the input saturation occurs. Now, if the difference of input $\triangle u_{\tau i}$ is infinite, the system becomes out of control. Therefore, the difference of input $\triangle u_{\tau i}$ is assumed to be bounded.*

$$|\triangle u_{\tau i}| \leq \zeta_i \tag{3.9}$$

The following auxiliary system is constructed for each subsystem of rotational

dynamics of the quadrotor system.

$$\begin{aligned}\begin{bmatrix}\dot{\chi}_{1j}\\ \dot{\chi}_{2j}\end{bmatrix} &= \begin{bmatrix}-c_{1j} & 1\\ 0 & -c_{2j}\end{bmatrix}\begin{bmatrix}\chi_{1j}\\ \chi_{2j}\end{bmatrix} + \begin{bmatrix}0\\ 1\end{bmatrix}\triangle u_{\tau j}\\ &= A_\chi \chi + B_\chi \triangle u_{\tau j}\end{aligned} \tag{3.10}$$

where c_{1i} and c_{2i} are positive constants, and χ_{1i} and χ_{2i} are the outputs of the auxiliary system.

Remark 3.1. *Note that if no input saturation exists, the auxiliary system does not affect the control input and the system stability.*

Again, the control design is based on backstepping with asymmetric BLF. Let us define the new parameters as

$$s_{1i} = r_{1i} - r_{di} - \chi_{1i},\ s_{2i} = r_{2i} - \beta_i - \chi_{2i}, \quad i = \phi, \theta, \psi \tag{3.11}$$

where r_{di} are the desired Euler angles, and β_i are the virtual control inputs. The controller design process is given as follows:

Step 1:Define the Log-BLF as follows:

$$V_{1i} = \frac{p(s_{1i})}{2}\log\left(\frac{\rho_{1bi}^2}{\rho_{1bi}^2 - s_{1i}^2}\right) + \frac{1-p(s_{1i})}{2}\log\left(\frac{\rho_{1ai}^2}{\rho_{1ai}^2 - s_{1i}^2}\right) + \frac{1}{2}\chi_{1i}^2 \tag{3.12}$$

where

$$\begin{aligned}\rho_{1ai} &:= r_{di} + \chi_{1i} + \rho_{1i}\\ \rho_{1bi} &:= \rho_{1i} - r_{di} - \chi_{1i}\end{aligned} \tag{3.13}$$

$$p(\cdot) = \begin{cases} 1, & \cdot > 0 \\ 0, & \cdot \leq 0 \end{cases} \tag{3.14}$$

With the following error coordinate changes,

$$\xi_{1ai} = \frac{s_{1i}}{\rho_{1ai}}, \quad \xi_{1bi} = \frac{s_{1i}}{\rho_{1bi}}, \quad \xi_{1i} = p(s_{1i})\xi_{1bi} + (1 - p(s_{1i}))\xi_{1ai} \tag{3.15}$$

The BLF in Eq. (3.12) can be rewritten as a following simple form.

$$V_{1i} = \frac{1}{2}\log\left(\frac{1}{1-\xi_{1i}^2}\right) + \frac{1}{2}\chi_{1i}^2 \tag{3.16}$$

Differentiating V_{1i} and using Eq. (3.10) in the resulting equation yield.

$$\begin{aligned} \dot{V}_{1i} \quad =& \frac{p(s_{1i})\xi_{1bi}}{\rho_{1bi}(1-\xi_{1bi}^2)}\left(s_{2i} + \beta_i - \dot{r}_{di} + c_{1i}\chi_{1i} - s_{1i}\frac{\dot{\rho}_{1bi}}{\rho_{1bi}}\right) \\ &+ \frac{(1-p(s_{1i}))\xi_{1ai}}{\rho_{1ai}(1-\xi_{1ai}^2)}\left(s_{2i} + \beta_i - \dot{r}_{di} + c_{1i}\chi_{1i} - s_{1i}\frac{\dot{\rho}_{1ai}}{\rho_{1ai}}\right) + \chi_{1i}\dot{\chi}_{1i} \end{aligned} \tag{3.17}$$

Define β_i as

$$\beta_i = -(k_{1i} + \bar{k}_{1i}(t))s_{1i} + \dot{r}_{di} - c_{1i}\chi_{1i} \tag{3.18}$$

where $\bar{k}_{1i}(t)$ is given by

$$\bar{k}_{1i}(t) = \sqrt{\left(\frac{\dot{\rho}_{1ai}}{\rho_{1ai}}\right)^2 + \left(\frac{\dot{\rho}_{1bi}}{\rho_{1bi}}\right)^2 + \kappa_i} \tag{3.19}$$

where $\kappa_i > 0$ ensures that the time derivative of β_i is nonzero even when $\dot{\rho}_{1ai}$ and $\dot{\rho}_{1bi}$ are both zeros.

Step 2: Define the Log-BLF as follows:

$$V_{2i} = V_{1i} + \frac{p(s_{2i})}{2}\log\left(\frac{\rho_{2bi}^2}{\rho_{2bi}^2 - s_{2i}^2}\right) + \frac{1-p(s_{2i})}{2}\log\left(\frac{\rho_{2ai}^2}{\rho_{2ai}^2 - s_{2i}^2}\right) + \frac{1}{2}\chi_{2i}^2 \tag{3.20}$$

where

$$\begin{aligned} \rho_{2ai} &:= \beta_i + \chi_{2i} + \rho_{2i} \\ \rho_{2bi} &:= \rho_{2i} - \beta_i - \chi_{2i} \end{aligned} \tag{3.21}$$

and

$$\xi_{2ai} = \frac{s_{2i}}{\rho_{2ai}}, \quad \xi_{2bi} = \frac{s_{2i}}{\rho_{2bi}}, \quad \xi_{2i} = p(s_{2i})\xi_{2bi} + (1-p(s_{2i}))\xi_{2ai} \tag{3.22}$$

Design control input $u_{\tau i}$ as

$$u_{\tau i} = -r_{3i} + \dot{\beta}_i - (k_{2i} + \bar{k}_{2i})s_{2i} - \mu_i s_{1i} - c_{2i}\chi_{2i} \tag{3.23}$$

where

$$\mu_i = \frac{p(s_{1i})}{\rho_{1bi}^2 - s_{1i}^2} + \frac{1-p(s_{1i})}{\rho_{1ai}^2 - s_{1i}^2} \tag{3.24}$$

and

$$\bar{k}_{2i}(t) = \sqrt{\left(\frac{\dot{\rho}_{2ai}}{\rho_{2ai}}\right)^2 + \left(\frac{\dot{\rho}_{2bi}}{\rho_{2bi}}\right)^2 + \kappa_i} \tag{3.25}$$

Using (2.18), (3.17), (3.18), (3.23), and Lemma 2, the time derivative of V_{2i} can be represented as

$$\dot{V}_{2i} \leq -k_{1i}\frac{\xi_{1i}^2}{1-\xi_{1i}^2} - k_{2i}\frac{\xi_{2i}^2}{1-\xi_{2i}^2} - c_{1i}\chi_{1i}^2 - c_{2i}\chi_{2i}^2 + \chi_{1i}\chi_{2i} + \chi_{2i}\triangle u_{\tau i} \tag{3.26}$$

From Eq. (3.9), the following inequalities hold.

$$\begin{aligned} \chi_{1i}\chi_{2i} &\leq \frac{1}{2}\chi_{1i}^2 + \frac{1}{2}\chi_{2i}^2 \\ \chi_{2i}\triangle u_{\tau i} &\leq \frac{1}{2}\chi_{2i}^2 + \frac{1}{2}\triangle u_{\tau i}^2 \leq \frac{1}{2}\chi_{2i}^2 + \frac{1}{2}\zeta_i^2 \end{aligned} \tag{3.27}$$

Equation (3.26) satisfies the following inequality:

$$\begin{aligned} \dot{V}_{2i} \leq & -k_{1i}\frac{\xi_{1i}^2}{1-\xi_{1i}^2} - k_{2i}\frac{\xi_{2i}^2}{1-\xi_{2i}^2} \\ & - \left(c_{1i} - \frac{1}{2}\right)\chi_{1i}^2 - (c_{2i}-1)\chi_{2i}^2 + \frac{1}{2}\zeta_i^2 \\ \leq & -\gamma_i V_{2i} + C_i \end{aligned} \tag{3.28}$$

where $c_{1i} > 1/2$, $c_{2i} > 1$, $\gamma_i = \min\{2k_{1i}, 2k_{2i}, 2(c_{1i}-1/2), 2(c_{2i}-1)\}$, and $C_i = \zeta_i^2/2$.

Theorem 3.2. *Consider the rotational dynamics of the quadrotor (2.18) with control input (3.23) and observer (2.20), and Assumptions 2.1 and 3.1. If the initial condition satisfies $|r_{1i}(0)| < \rho_{1i}$ and $|r_{2i}(0)| < \rho_{2i}$, the symmetric constant constraint is not violated, i.e., $|r_{1i}(t)| < \rho_{1i}$ and $|r_{2i}(t)| < \rho_{2i}$, and the closed-loop signals z_{1i}, z_{2i}, χ_{1i}, and χ_{2i} will be uniformly bounded.*

Proof. The initial condition requirement is equivalent to $-\rho_{1aj}(0) < s_{1j}(0) < \rho_{1bj}(0)$ and $-\rho_{2aj}(0) < s_{2j}(0) < \rho_{2bj}(0)$. Then, Lemma 2.1 ensures that $|\xi_{1j}(t)| < 1$ and $|\xi_{2j}(t)| < 1$, $\forall t > 0$. At the same time, from Assumption 3.1 and Eq. (3.10), χ_{1j}, and χ_{2j} are all bounded as A_χ is Hurwitz.

Taking the integral of Eq. (3.28) yields $0 \leq V_{2j}(t) \leq \left(V_{2j}(0) - \frac{C_j}{\gamma_j}\right)e^{-\gamma_j t} + \frac{C_j}{\gamma_j} \leq V_{2j}(0) + \frac{C_j}{\gamma_j}$, $\forall t > 0$, which leads to

$$\frac{1}{2}\log\left(\frac{1}{1-\xi_{1j}^2}\right) \leq V_{2j}(0) + \frac{C_j}{\gamma_j} \tag{3.29}$$

Taking the exponent arithmetic on both sides and reformulating the resulting equation with Eq. (3.15), we have

$$-\rho_{1aj}\sqrt{1-e^{-2(V_{2j}(0)+C_j/\gamma_j)}} \leq s_{1j} \leq \rho_{1bj}\sqrt{1-e^{-2(V_{2j}(0)+C_j/\gamma_j)}} \tag{3.30}$$

for all $t > 0$. In a similar way, we have

$$-\rho_{2aj}\sqrt{1-e^{-2(V_{2j}(0)+C_j/\gamma_j)}} \leq s_{2j} \leq \rho_{2bj}\sqrt{1-e^{-2(V_{2j}(0)+C_j/\gamma_j)}} \tag{3.31}$$

In Eqs. (3.30) and (3.31), it can be shown that $-\rho_{1aj} < s_{1j} < \rho_{1bj}$ and $-\rho_{2aj} < s_{2j} < \rho_{2bj}$. With Eqs. (3.11), (3.13), and (3.21), the following inequalities can be inferred.

$$-\rho_{1j} < r_{1j} < \rho_{1j}, \quad -\rho_{2j} < r_{2j} < \rho_{2j} \tag{3.32}$$

□

Chapter 4

Practical Guideline for Gain Tuning

4.1 Analogy of Proposed Controller to PD Controller

This section presents the analogy between the proposed controller and PD controller. The proposed control input can be formulated as the PD-like form so that the control gain parameters can be properly chosen.

4.1.1 Position Tracking Controller

Let us consider the position tracking control system. Substituting $z_{1i} = e_{1i}/\rho_i$, $z_{2i} = e_{2i} - \alpha_i$, and $\alpha_i = \dot{\rho}_i z_{1i} - \rho_i k_{1i} z_{1i}$ into Eq. (3.4) yields:

$$q_i = -k_{Pi} e_{1i} - k_{Di} e_{2i} - e_{3i}, \quad i = x, y, z \tag{4.1}$$

where

$$k_{Pi} = -\left(\frac{\ddot{\rho}_i}{\rho_i} - \frac{\dot{\rho}_i^2}{\rho_i^2} - \frac{1}{\rho_i^2 - e_{1i}^2} + \frac{k_{2i}\dot{\rho}_i}{\rho_i} \right) + k_{1i} k_{2i} \tag{4.2a}$$

$$k_{Di} = -\frac{\dot{\rho}_i}{\rho_i} + (k_{1i} + k_{2i}) \tag{4.2b}$$

Now, the control law (4.1) can be seen as the combination of an error-based PD feedback components with gains k_{Pi} and k_{Di}, and disturbance compensation component. The PD-like gains, k_{Pi} and k_{Di}, should be positive. Due to the definition of ρ_i,

$-\ddot{\rho}_i/\rho_i + \dot{\rho}_i^2/\rho_i^2 > 0$, and Eq. (3.1) with $\dot{\rho}_i/\rho_i < 0$, $k_{2i} > 0$, k_{Pi} is always positive. Also, $\dot{\rho}_i/\rho_i < 0$ makes $k_{1i}, k_{2i} > 0$, k_{Di} always positive.

In case of e_{1i} goes to 0 and t goes to ∞, i.e., steady state, the first term of k_{Pi} and k_{Di} goes to $1/\rho_{\infty i}^2$ and 0, respectively. Then, the control gains can be approximated as follows:

$$k_{Pi} \approx k_{1i}k_{2i} + \frac{1}{\rho_{\infty i}^2}, \quad k_{Di} \approx k_{1i} + k_{2i} \tag{4.3}$$

4.1.2 Attitude Controller

Let us consider the attitude control system. Substituting s_{1i} and s_{2i} in Eq. (3.11), and β_i in Eq. (3.18) into Eq. (3.23) yields

$$u_{\tau i} = -k_{Pi}e_{1i} - k_{Di}e_{2i} - r_{3i} + \ddot{r}_{di} + l_i(\chi_{1i}, \chi_{2i}), \quad i = \phi, \theta, \psi \tag{4.4}$$

where $e_{1i} = r_{1i} - r_{di}$, $e_{2i} = r_{2i} - \dot{r}_{di}$,

$$\begin{aligned} l_i(\chi_{1i}, \chi_{2i}) =& \Big((k_{1i} + \bar{k}_{1i})(k_{2i} + \bar{k}_{2i}) - (k_{1i} + \bar{k}_{1i})c_{1i} - (k_{2i} + \bar{k}_{2i})c_{1i} \\ & + \mu_i + \dot{\bar{k}}_{1i} + c_{1i}^2 \Big)\chi_{1i} \\ & + \Big(-(k_{2i} + \bar{k}_{2i}) - 2c_{1i} \Big)\chi_{2i} \end{aligned} \tag{4.5}$$

and

$$\begin{aligned} k_{Pi} =& \ \dot{\bar{k}}_{1i} + \mu_i + (k_{1i} + \bar{k}_{1i})(k_{2i} + \bar{k}_{2i}) \\ k_{Di} =& \ (k_{1i} + \bar{k}_{1i}) + (k_{2i} + \bar{k}_{2i}) \end{aligned} \tag{4.6}$$

Similarly, the control law (4.4), can now be seen as a combination of an error-based PD feedback component with gains k_{Pi} and k_{Di}, disturbance compensation component, model reference compensation component, and input saturation compensation component. The PD-like gains, k_{Pi} and k_{Di}, should be positive. Assume that input

saturation does not occur, $\chi_{1i} = 0$ and $\chi_{2i} = 0$. Then k_{Pi} and k_{Di} are always positive value. Especially, in case of e_{1i} and e_{2i} go to 0, the control gains can be approximated as follows:

$$k_{Pi} \approx k_{1i}k_{2i} + (k_{1i} + k_{2i})\sqrt{\kappa_i} + \kappa_i, \quad k_{Di} \approx k_{1i} + k_{2i} + 2\sqrt{\kappa_i} \tag{4.7}$$

4.2 Analogy of Modified Controller to PID Control

This section presents the analogy of the proposed controller to the PID controller. By adding additional integral action to the proposed control input, the controller proposed in Chapter 3 can be changed to the PID-like form, so that the control gain parameter can be properly chosen. The tuning guideline for both position tracking and attitude controllers are given and a mathematical analysis of control parameters is shown below.

4.2.1 Position Tracking Controller

The position tracking virtual control input α_i can be modified as:

$$\alpha_i = \dot{\rho}_i z_{1i} - \rho_i k_{1i} z_{1i} - k_{3i}\rho^2(1 - z_{1i}^2)\int e_{1i}dt, \quad i = x, y, z \tag{4.8}$$

Theorem 4.1. *Consider the position error dynamics of the quadrotor (2.17) with control input (3.4) with α in (4.8), observer (2.19), and Assumption 2.1. If the initial condition satisfies $|e_{1i}(0)| < \rho_i(0)$, the symmetric time-varying constraint is not violated, i.e., $|e_{1i}(t)| < \rho_i(t)$ for all $t > 0$, and the closed-loop signals z_{1i} and z_{2i} are uniformly bounded.*

Proof. From the initial condition requirement, Lemma 2.1 ensures that $|z_{1i}(t)| < 1$, which means $|e_{1i}(t)| < \rho_i(t)$. Consider the following barrier-Lyapunov function:

$$V_i = \frac{1}{2}\log\left(\frac{1}{1 - z_{1i}^2}\right) + \frac{1}{2}z_{2i}^2 + \frac{1}{2}k_{3i}\left(\int e_{1i}dt\right)^2 \tag{4.9}$$

Then, the time derivative of V_i satisfies the following inequality equation:

$$\dot{V}_i \leq -\gamma_i V_i + C_i \tag{4.10}$$

where $\gamma_i = \min\{2k_{1i}, 2k_{2i}\}$, and $C_i = k_{2i}k_{3i}\left(\int e_{1i}dt\right)^2/2$. Integrating both side of the inequality of Eq. (4.10) $0 \leq V_i(t) \leq \left(V_i(0) - \frac{C_i}{\gamma_i}\right)e^{-\gamma_i t} + \frac{C_i}{\gamma_i} \leq V_i(0) + \frac{C_i}{\gamma_i}$, $\forall t > 0$, which leads to:

$$\frac{1}{2}\log\left(\frac{1}{1-z_{1i}^2}\right) \leq V_i(0) + \frac{C_i}{\gamma_i} \tag{4.11}$$

Taking the exponent arithmetic on both sides and reformulation yield:

$$|z_{1i}| \leq \sqrt{1 - e^{-2(V_i(0)+C_i/\gamma_i)}} < 1, \quad \forall t > 0 \tag{4.12}$$

Furthermore, since $\frac{1}{2}z_{2i}^2 \leq V_i(0) + \frac{C_i}{\gamma_i}$, it can be shown that $||z_{2i}|| \leq \sqrt{2(V_i(0) + \frac{C_i}{\gamma_i})}$, $\forall t > 0$. □

Substituting z_{1i}, z_{2i}, and α_i in Eq. (4.8) into Eq. (3.4) yields:

$$q_i = -k_{Pi_m}e_{1i} - k_{Di_m}e_{2i} - k_{Ii_m}\int e_{1i}dt - e_{3i} + 2k_{3i}e_{1i}e_{2i}\int e_{1i}dt \tag{4.13}$$

where

$$\begin{aligned} k_{Pi_m} &= k_{Pi} + k_{3i}(1 - z_{1i}^2)\rho^2 \\ k_{Di_m} &= k_{Di} \\ k_{Ii_m} &= 2k_{3i}\rho_i\dot{\rho}_i + (1 - z_{1i}^2)k_{2i}k_{3i}\rho_i^2. \end{aligned} \tag{4.14}$$

The control law (4.13) now becomes a combination of error-based PID feedback component with gains k_{Pi_m}, k_{Di_m}, and k_{Ii_m}, and disturbance compensation component. Note that k_{Pi_m} and k_{Di_m} are always positive. If the following inequalities hold, the integral control gain, k_{Ii_m}, is guaranteed to be positive for $t \geq 0$.

$$(\rho_i^2 - e_{1i}^2)k_{2i} + 2\rho_i\dot{\rho}_i > 0. \tag{4.15}$$

This implies that k_{2i} needs to be large enough to make k_{Ii_m} be positive.
In case of e_{1i} and e_{2i} go to 0, the second term of k_{Pi_m} goes to $k_{3i}\rho_{\infty i}^2$ and the first term of k_{Ii_m} goes to 0 as $t \to \infty$. Then, the control gains can be approximated as follows:

$$k_{Pi_m} \approx k_{1i}k_{2i} + k_{3i}\rho_{\infty i}^2 + \frac{1}{\rho_{\infty i}^2}, \quad k_{Di_m} \approx k_{1i} + k_{2i}, \quad k_{Ii_m} \approx k_{2i}k_{3i}\rho_{\infty i}^2. \tag{4.16}$$

By solving the following third-order equation with respect to k_{2i}, which is derived from Eq. (4.16), the set of equivalent k_{1i}, k_{2i}, and k_{3i} gains can be deterimined as follows:

$$\begin{aligned} &k_{2i}^3 - k_{Di_m}k_{2i}^2 + \left(k_{Pi_m} - \frac{1}{\rho_{\infty i}^2}\right)k_{2i} - k_{Ii_m} = 0 \\ &k_{1i} = k_{Di_m} - k_{2i} \\ &k_{3i} = \frac{1}{k_{2i}\rho_{\infty i}^2}k_{Ii_m}. \end{aligned} \tag{4.17}$$

Equation (4.15) represents conditions that guarantee PID gains of Eq. (4.14) positive, and Eq. (4.17) provides the analogy of the proposed controller to the PID gains.

To investigate the meaning of Eq. (4.17), the result with $k_{Pi_m} = 60$ and $k_{Ii_m} = 1$ is presented in Fig. 4.1a), and with $k_{Di_m} = 50$ and $k_{Ii_m} = 1$ is presented in Fig. 4.1b), where $\rho_{0i} = 1$m, $\rho_{\infty i} = 0.5$m, $\rho_{ki} = 0.5$, $\rho_{1i} = 45$deg, and $\rho_{1i} = 100$deg/s.

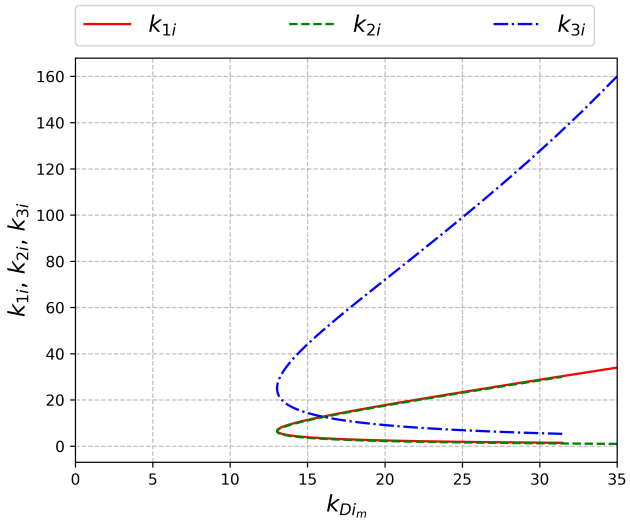

(a) $k_{Pi_m} = 60$ and $k_{Ii_m} = 1$

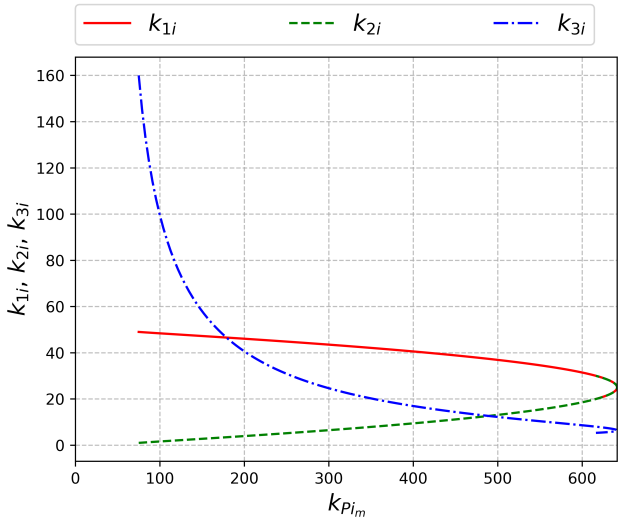

(b) $k_{Di_m} = 50$ and $k_{Ii_m} = 1$

Figure 4.1: Coupled controller gains, k_{1i}, k_{2i}, and k_{3i}, for specific k_{Pi_m}, k_{Di_m}, and k_{Ii_m}. (Position tracking controller)

Remark 4.1. *Tuning Guideline for position tracking controller*

1. *For a given value of k_{Pi_m}, the k_{1i}, k_{2i}, and k_{3i} values can be determined for any desired value of k_{Di_m}.*

2. *For a given value of k_{Di_m}, the k_{1i}, k_{2i}, and k_{3i} values can be determined for any desired value of k_{Pi_m}.*

3. *Since k_{Di_m} is the summation of k_{1i} and k_{2i}, one of their values determines the other.*

4. *Selecting too small value of k_{2i} can make $k_{Ii_m} < 0$, which makes whole system unstable, due to Eq. (4.15).*

Remark 4.2. *Note that the parameters for prescribed performances, ρ_{0i}, $\rho_{\infty i}$, and ρ_{ki}, also affect the PID gains. If these values vary, feasible solutions to Eq. (4.15) and k_{Pi_m}, k_{Di_m}, and k_{Ii_m} will also change. In Eq. (4.16), we can see that the proportional and integral gains of the proposed controller are changed when $\rho_{\infty i}$ change. The proportional gain k_{Pm_i} significantly increases when $\rho_{\infty i}$ goes to 0, which is a tighter performance criterion. This means that if we want less tracking error, the value of gains k_{1i} and k_{2i} should be decreased to keep the value of k_{Pm_i}. Similarly, the integral gain decreases when $\rho_{\infty i}$ decreases so that the k_{3i} should be chosen properly to keep the desired integral gain value.*

Remark 4.3. *By approximating the proposed control gain to PID-like gain considering asymptotic tracking performance, it can be expected that $\mathbf{e}_{1(\cdot)}$ and $\mathbf{e}_{2(\cdot)}$ go to 0 and $t \to \infty$. However, at the beginning of the control, control inputs are relatively vulnerable to the prescribed performance bound ρ_i. Note that the initial gain effects can be made small by selecting suitable performance bound. For example, consider*

an integral gain in Eq. (4.14). When $t = 0$, $k_{Ii_m}(0) = -2k_{3i}\rho_{0i}\rho_{ki}(\rho_{0i} - \rho_{\infty i})$. *By selecting small* ρ_{ki}, $\rho_{\infty i}$, *or* $\rho_{0i} - \rho_{\infty i}$, *the effect of the ignored terms can be decreased.*

4.2.2 Attitude Controller

Now, let us consider an attitude controller. The attitude virtual control input β_i can be modified as:

$$\beta_i = -(k_{1i} + \bar{k}_{1i}(t))s_{1i} + r_{di} - c_{1i}\chi_{1i} - k_{3i}(1 - \xi_{1i}^2)\int e_{1i}dt, \quad i = \phi, \theta, \psi \tag{4.18}$$

Theorem 4.2. *Consider the rotational dynamics of the quadrotor (2.18) with control input (3.23) with* β_i *in (4.18), observer (2.20), and Assumptions 2.1 and 3.1. If the initial condition satisfies* $|r_{1i}(0)| < \rho_{1i}$ *and* $|r_{2i}(0)| < \rho_{2i}$, *the symmetric constant constraint is not violated, i.e.,* $|r_{1i}(t)| < \rho_{1i}$ *and* $|r_{2i}(t)| < \rho_{2i}$, *and the closed-loop signals* s_{1i}, s_{2i}, χ_{1i}, *and* χ_{2i} *will be uniformly bounded.*

Proof. From the initial condition requirement, Lemma 2.1 ensures that $|\xi_{1i}(t)| < 1$ and $|\xi_{2i}(t)| < 1$, $\forall t$, and at the same time, from Assumption 3.1 and Eq. (3.10), χ_{1j}, and χ_{2j} are all bounded as A_χ is Hurwitz.

$$V_i = V_{2i} + \frac{1}{2}k_{3i}\left(\int e_{1i}dt\right)^2 \tag{4.19}$$

Then, the time derivative of V_i satisfies the following inequality equation:

$$\dot{V}_i \leq -\gamma_i V_i + C_i \tag{4.20}$$

where $\gamma_i = \min\{2k_{1i}, 2k_{2i}, 2(c_{1i} - 1/2), 2(c_{2i} - 1)\}$, and $C_i = \zeta_i^2/2 + k_{2i}k_{3i}\left(\int e_{1i}dt\right)^2/2$. The rest of the proof is the same as the proof of Theorem 3.2. □

Substituting s_{1i}, s_{2i}, and β_i in Eq. (4.18) into Eq. (3.23) yields:

$$\begin{aligned} u_{\tau i} &= -k_{Pi_m} e_{1i} - k_{Di_m} e_{2i} - k_{Ii_m} \int e_{1i} dt - r_{3i} \\ &\quad + l_i(\chi_{1i}, \chi_{2i}) + (k_{2i} + \bar{k}_{2i})\dot{r}_{1i} - (k_{1i} + \bar{k}_{1i})\ddot{r}_{1i} + 2k_{3i}\xi_{1i}\xi_{2i} \int e_{1i} dt \end{aligned} \tag{4.21}$$

where

$$\begin{aligned} k_{Pi_m} &= k_{Pi} + k_{3i}(1 - \xi_{1i}^2) \\ k_{Di_m} &= k_{Di} \\ k_{Ii_m} &= (k_{2i} + \bar{k}_{2i})k_{3i}(1 - \xi_{1i}^2). \end{aligned} \tag{4.22}$$

Similarly, the control law (4.21), can now be understood as a combination of an error-based PID feedback component with gains k_{Pi_m}, k_{Di_m}, and k_{Ii_m}, disturbance compensation component, and input saturation compensation component. The second term of k_{Pi_m} and k_{Ii_m} are always positive, and therefore all PID-like gains are always positive. Assume that input saturation does not occur, and e_{1i} and e_{2i} go to 0, then the control gains can be approximated as follows:

$$\begin{aligned} k_{Pi_m} &\approx k_{1i}k_{2i} + k_{3i} + (k_{1i} + k_{2i})\sqrt{\kappa_i} + \kappa_i \\ k_{Di_m} &\approx k_{1i} + k_{2i} + 2\sqrt{\kappa_i} \\ k_{Ii_m} &\approx (k_{2i} + \sqrt{\kappa_i})k_{3i}. \end{aligned} \tag{4.23}$$

By solving the following third-order equation with respect to k_{2i}, which is derived from Eq. (4.23), the set of equivalent k_{1i}, k_{2i}, and k_{3i} gains can be determined as

follows:

$$\begin{aligned} & k_{2j}^3 - (k_{Dj_m} - 3\sqrt{\kappa_j})k_{2j}^2 \left(k_{Pj_m} - 2k_{Dj_m}\sqrt{\kappa_j} + 3\kappa_j\right) k_{2j} \\ & \quad + (k_{Pj_m}\sqrt{\kappa_j} - k_{Dj_m}\kappa_j - k_{Ij_m} + \kappa_j\sqrt{\kappa_j}) = 0 \\ & k_{1j} = k_{Dj_m} - k_{2j} - 2\sqrt{\kappa_j} \\ & k_{3j} = \frac{1}{k_{2j} + \sqrt{\kappa_j}} k_{Ij_m}. \end{aligned} \tag{4.24}$$

Equation (4.24) represents relations between PID gains and controller gains.

To investigate the meaning of Eq. (4.24), the result with $k_{Pi_m} = 100$ and $k_{Ii_m} = 1$ is presented in Fig. 4.2a), and with $k_{Di_m} = 45$ and $k_{Ii_m} = 1$ is presented in Fig. 4.2b).

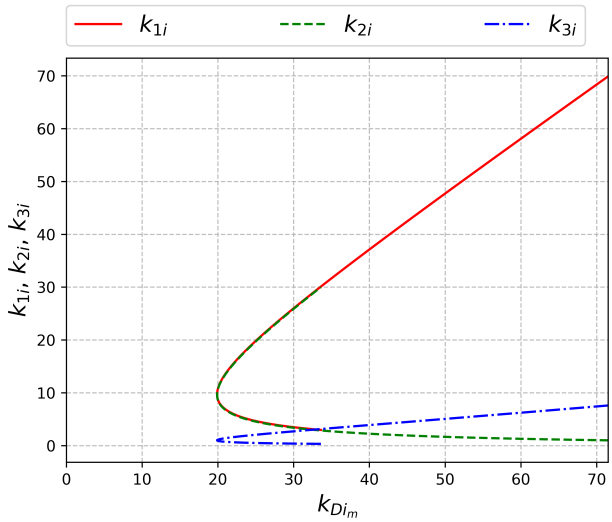

(a) $k_{Pi_m} = 100$ and $k_{Ii_m} = 1$

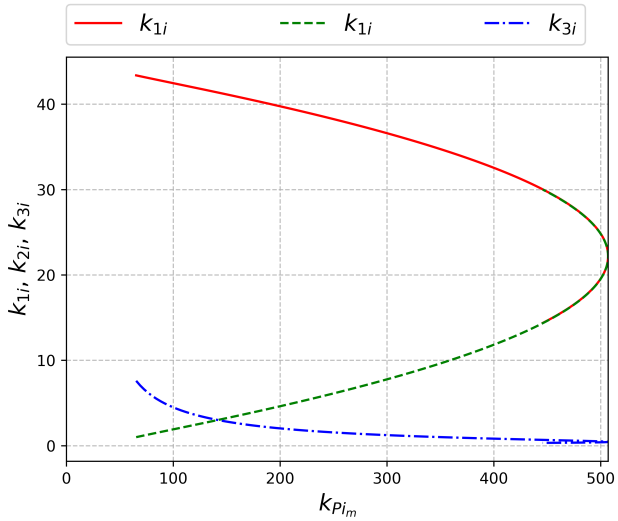

(b) $k_{Di_m} = 45$ and $k_{Ii_m} = 1$

Figure 4.2: Coupled controller gains, k_{1i}, k_{2i}, and k_{3i}, for specific k_{Pi_m}, k_{Di_m}, and k_{Ii_m}. (Attitude controller)

Remark 4.4. *Contents 1-3 in Remark 4.1 can also be used for attitude controller gain tuning.*

Remark 4.5. *Note that the prescribed performance bound ρ_{1i} influences the values of the PID-like gain. For the gain k_{Pi} of k_{Pi_m} in Eq. (4.23), the term μ_i, which is represented as Eq. (3.24), is inverse proportional to ρ_{1i}. Therefore, if the desired bound ρ_{1i} is too small, the gain k_{Pi_m} increases significantly. To compensate this effect, k_{1i} and k_{2i} should be decreased.*

Remark 4.6. *By approximating the proposed control gain to PID-like gain, it can be expected that $\mathbf{e}_{1(\cdot)}$ and $\mathbf{e}_{2(\cdot)}$ go to 0 and the input saturation does not occur. However, the term $\bar{k}_{2i}$ significantly changes i) at the beginning of the control, or ii) when the actuator fault occurs, because of the effect of the term $k_{1i}\dot{s}_{1i}$ in $\dot{\beta}_i$. The term $\dot{s}_{1i} = \dot{r}_{1i} - \dot{r}_{di}$ inevitably has nonzero value at the transient state of the control or at the time of the fault occurs. Therefore, with the gain k_{1i}, absolute value of $\dot{\beta}_i$ increases and the value of k_{Pi_m} and k_{Di_m} increases (See Eq. (4.24)). Note that, unlike the position tracking controller, the PID-like gain of the attitude control is only applied to the steady-state phase with exact fault information, not the transient phase.*

4.3 Guideline for ESO Parameter Tuning

This section analyzes the effect of changes in ESO gain parameters on control performance.

1. Increasing the observer gain l_i in Eq. (2.19) yields a faster estimation of state parameters and disturbances. However, because the magnitude of the peak is determined in proportion to the magnitude of the observer gain, the high observer gain may degrade the control performance in the case of a fault. There exists a trade-off between the estimation response time and the magnitude of peaking. For example, the peak of state variables may occur, which leads to the large control input. More specifically, if the observer gain of the position tracking controller is too large, the magnitude of the peak rapidly increases, resulting in an abrupt change of position tracking control input q_i, which yields big changes in desired Euler angles (see Eq. (2.16)). If the desired Euler angles increase and are close to the prescribed performance bounds ρ_{1i}, ρ_{1bi}(or ρ_{1ai}) becomes smaller (see Eq. (3.13)), resulting in large attitude control input $u_{\tau i}$. Therefore, it is recommended that the observer gain should be chosen less than a certain value in the position tracking controller.

2. Consider a_i's in Eq. (2.19), which are chosen such that Eq. (2.21) is Hurwitz. Increasing the absolute real value of the poles of the matrix Eq. (2.21) yields a faster estimation of the state parameters and disturbances, but the magnitude of the peak increases, yielding similar results as described in 1.

3. Consider δ in Eq. (2.22). Decreasing δ yields faster estimation, but the magnitude of the peak increases and the oscillation in the estimation may occur.

Chapter 5

Numerical Simulation

In this chapter, numerical simulation is performed to demonstrate the effectiveness of the proposed control method. The model parameters of the quadrotor used in the simulation are summarized in Table 5.1 [37]. The initial position and Euler angle values of the quadrotor for the simulation are set as $[0, 0, 0]^T$m and $[0, 0, 0]^T$deg, respectively.

Table 5.1: Quadrotor Parameters

Parameter	Name	Value
m	Mass	0.65kg
I_{xx}	Moment of inertial about x-axis	7.5×10^{-3}kgm^2
I_{yy}	Moment of inertial about y-axis	7.5×10^{-3}kgm^2
I_{zz}	Moment of inertial about z-axis	1.3×10^{-2}kgm^2
c_f	Thrust coefficient	3.13×10^{-5}Ns^2
c_τ	Drag moment coefficient	7.5×10^{-7}Ns^2
d	Arm length	0.23m
$\Omega_{\max}$	Maximum rotor speed	$1,000$rad/s

5.1 Case 1: Multiple Faults without ESO

First, to demonstrate the performance of the proposed BLF-based controller itself, the numerical simulation is performed without the use of ESO. The normal backstepping (BS) controller with two different gain settings is selected for comparison: i) the first one has the same control gains as the proposed controller, which is denoted as BS, and ii) the second one has tuned control gains, which is denoted as BS (tuned). Note that the tracking performance of BS (tuned) is better than that of BS. The reference trajectory is constructed as $\mathbf{p_d} = [1,\ \cos(t),\ -t]^T$. The scenario of actuator effectiveness losses are: 20% effectiveness in rotor 1 at 5 s and 50% effectiveness in rotor 2 at 7 s. In this simulation, ESOs are not used, and it is assumed that the fault detection is provided by a fault detection and identification module with a time delay of 0.2 s. The disturbance and model uncertainty are not considered.

The parameters of the proposed controller are selected as $k_{1i} = 0.1$, $k_{2i} = 6$, and $k_{3i} = 0$, for $i = x, y, z$, and $k_{1i} = 8$, $k_{2i} = 18.75$, and $k_{3i} = 0$, for $i = \phi, \theta, \psi$. The same gain parameters are used in BS. The predefined bounds for the position errors are selected as $\rho_{0i} = 1.5$, $\rho_{\infty i} = 0.2$, and $\rho_{k_i} = 1$, for $i = x, y, z$, so that the position error cannot exceed 0.2m even if actuator fault occurs. For Euler angles and angular rates, $\rho_{1i} = 45$ deg and $\rho_{2i} = 150$ deg/s, for $i = \phi, \theta$, and $\rho_{1i} = 45$ deg and $\rho_{2i} = 180$ deg/s for $i = \psi$. The parameters of the BS (tuned) are selected as $k_{1i} = 0.5$, $k_{2i} = 6$, and $k_{3i} = 0$, for $i = x, y, z$, and $k_{1i} = 8$, $k_{2i} = 18.75$, and $k_{3i} = 0$, for $i = \phi, \theta, \psi$.

The simulation results are shown in Figs. 5.1-5.5. As shown in Fig. 5.1, only the proposed controller maintains the prescribed position tracking bounds when the fault occurs. BS (tuned) maintains prescribed bounds before fault, but shows tracking error fluctuations when the first actuator fault occurs and the x position gets out of the bounds for a while. Figures 5.2-5.4 show the Euler angle, angular rate, and Euler angle tracking error histories, respectively. When the first fault occurs at 5 s, the angular rates of the proposed controller have been maintained within the system constraints. Meanwhile, as shown in Fig. 5.3, the pitch rate overshoot, which is bigger than the prescribed bounds, can be seen in both BS controllers. As shown in Fig. 5.4, the proposed method has oscillation and slow convergence rate in angular rate after the fault occurs, which will be treated by using the ESO. The control input signals are displayed in Fig. 5.5, and the fluctuations are shown when the fault occurs.

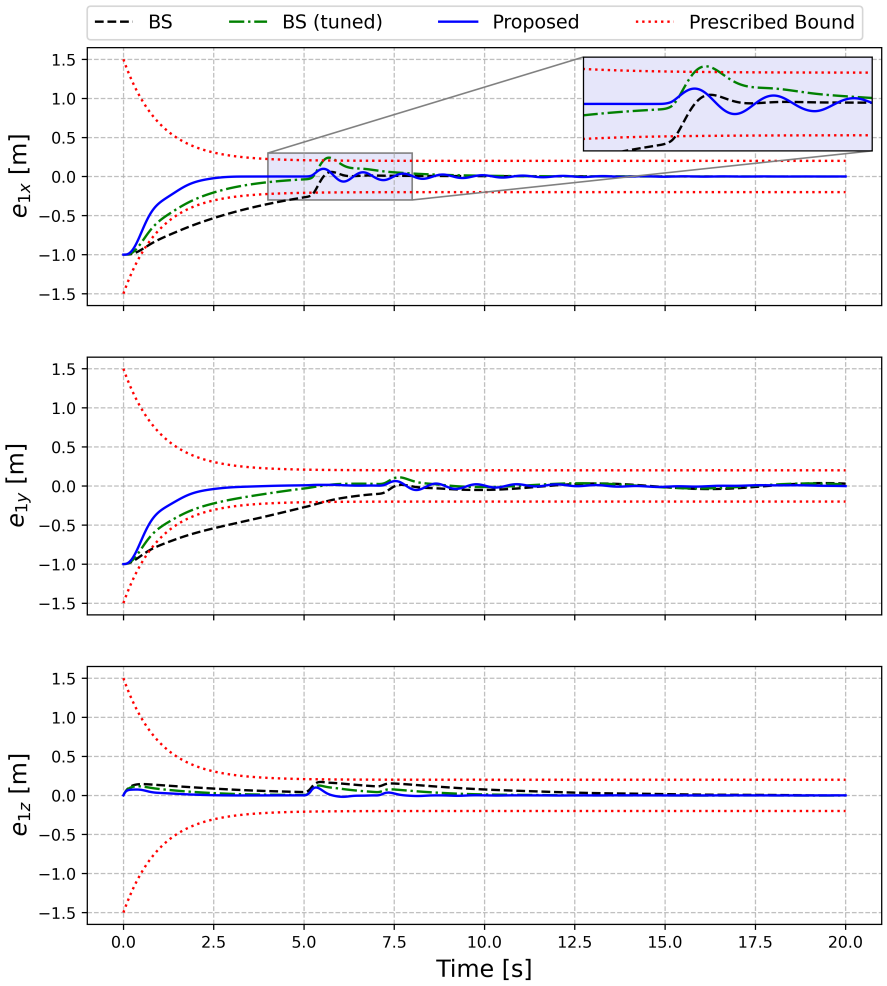

Figure 5.1: Position tracking error responses (Case 1)

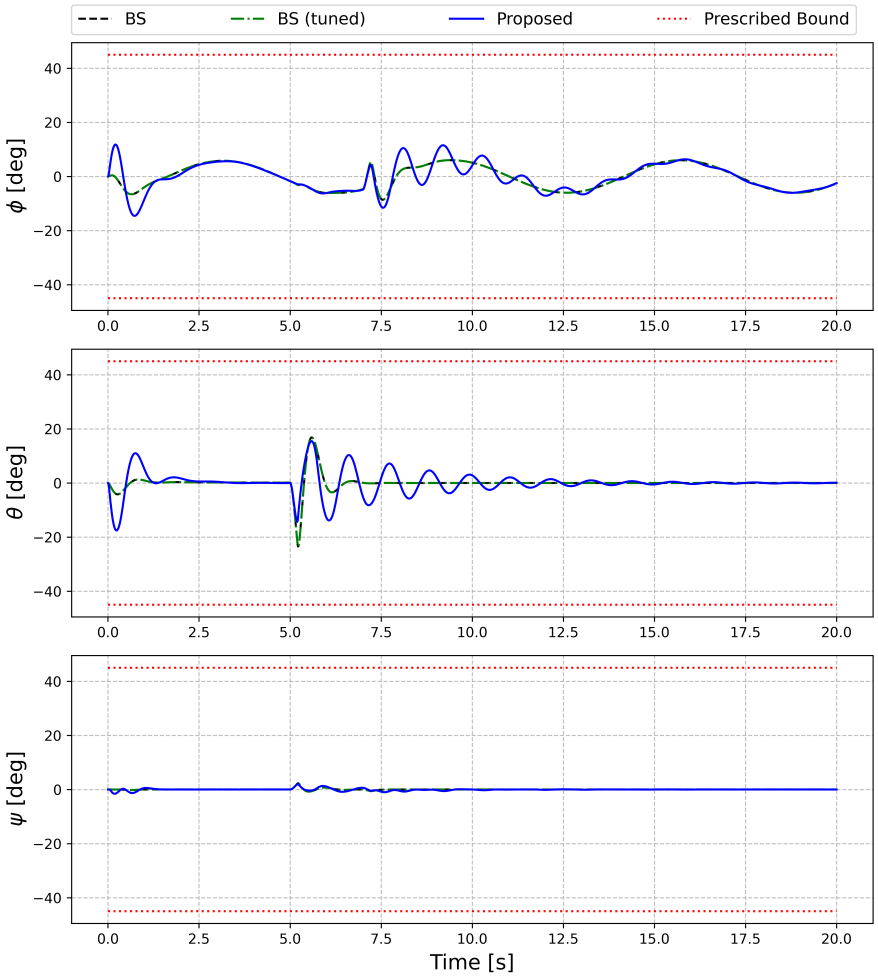

Figure 5.2: Euler angle responses (Case 1)

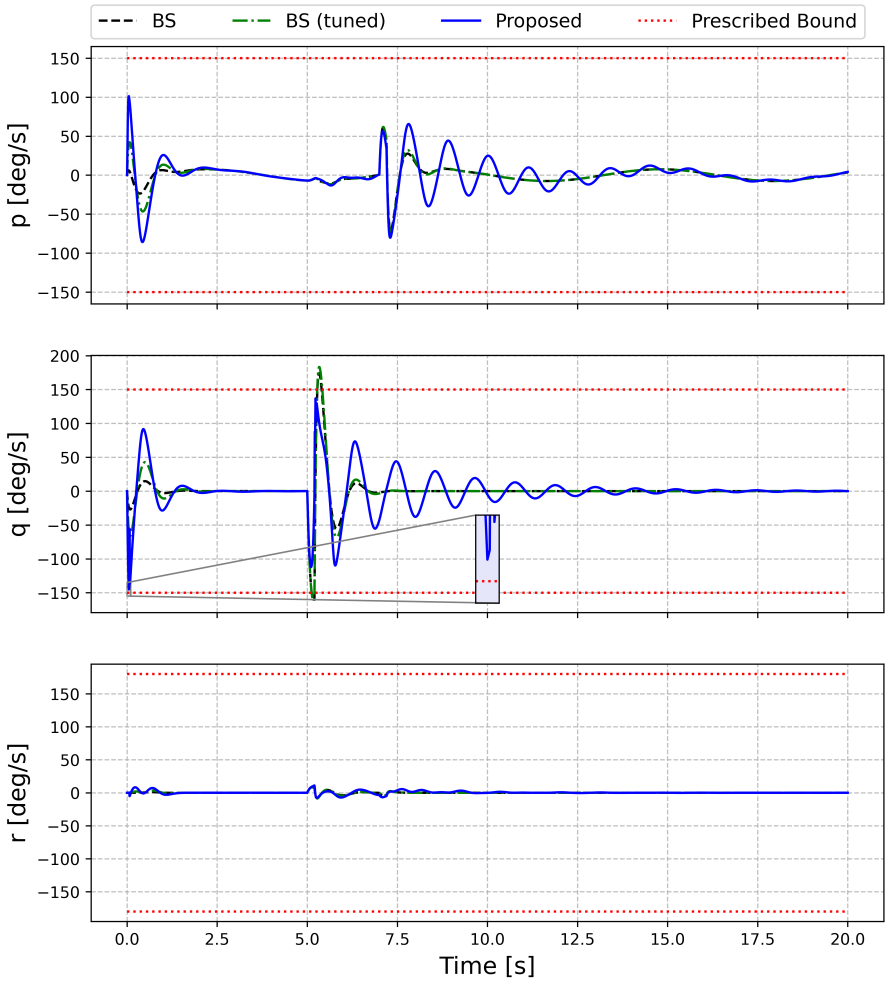

Figure 5.3: Angular rate responses (Case 1)

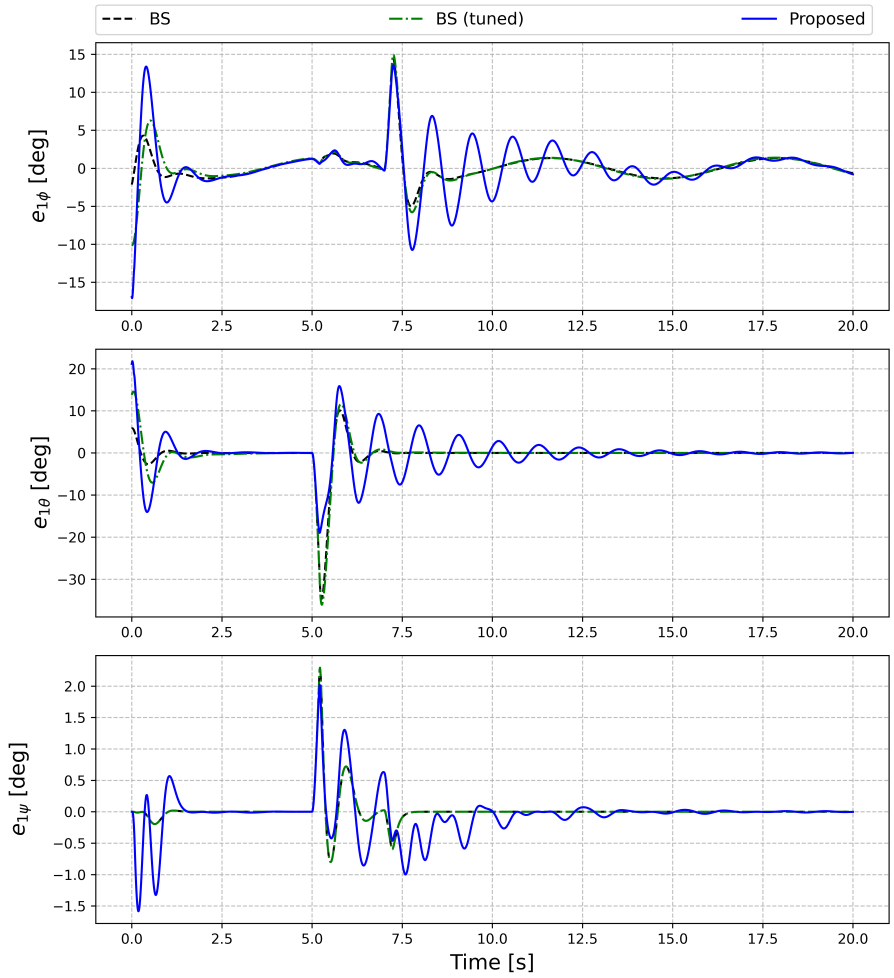

Figure 5.4: Euler angle tracking errors (Case 1)

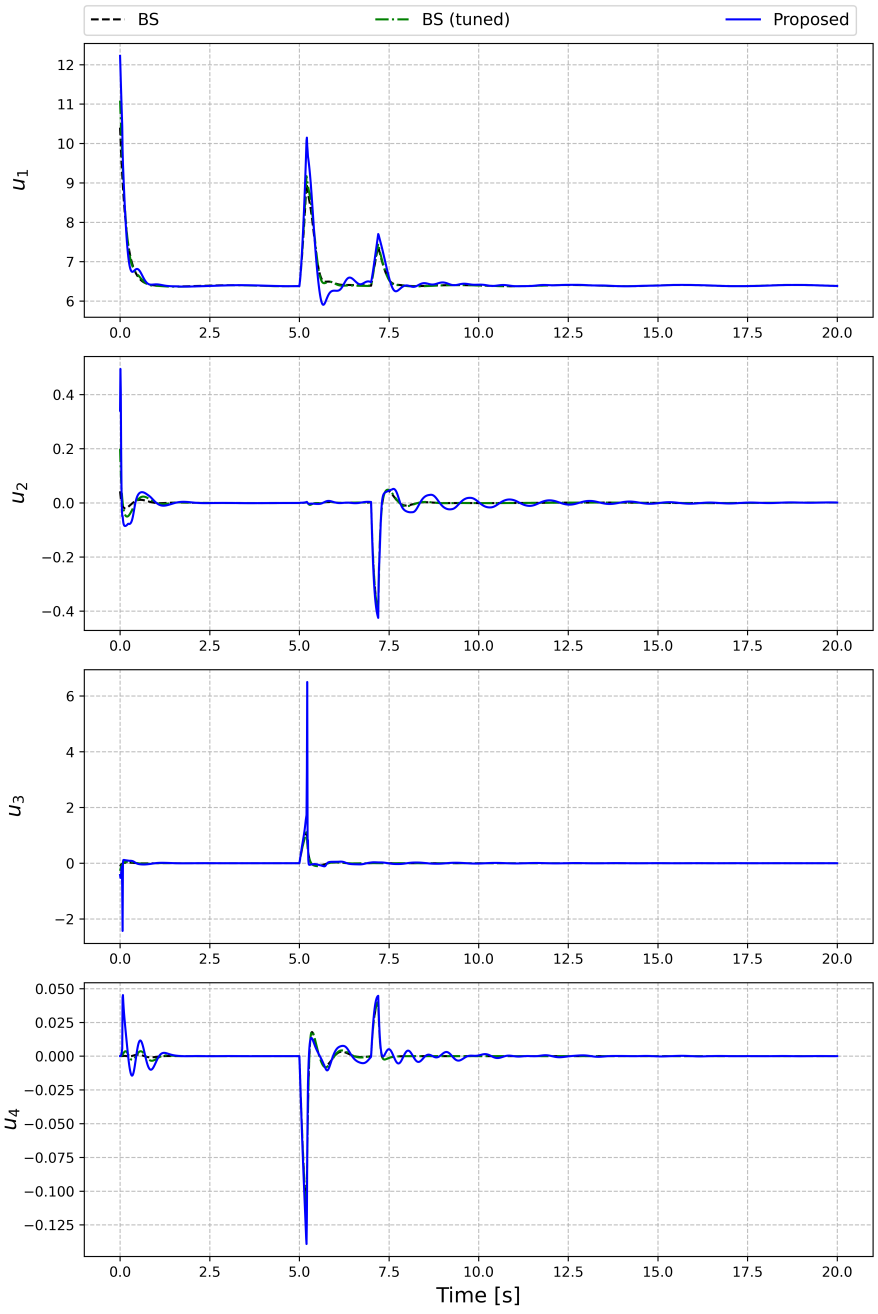

Figure 5.5: Control input responses (Case 1)

Table 5.2: The comparison of the STD (Case 1)

	Proposed	BS	BS (tuned)
e_{1x} [m]	**0.1675**	0.2748	0.2129
e_{1y} [m]	**0.1643**	0.2624	0.2014
e_{1z} [m]	**0.0182**	0.0508	0.0335
$e_{1\phi}$ [deg]	3.2414	**1.8608**	2.2052
$e_{1\theta}$ [deg]	4.1954	**3.7861**	4.3764
$e_{1\psi}$ [deg]	0.3516	**0.2190**	**0.2190**

Table 5.3: The comparison of the largest fluctuation (Case 1)

	Overshoot (fault 1)		
	Proposed	BS	BS (tuned)
e_{1x} [m]	**0.0981**	-	0.2408
e_{1y} [m]	**0.0142**	-	-0.0326
e_{1z} [m]	**0.1005**	0.1715	0.1255
$e_{1\phi}$ [deg]	2.3501	**1.9420**	2.1463
$e_{1\theta}$ [deg]	**-18.9789**	-34.6177	-36.0392
$e_{1\psi}$ [deg]	**2.0224**	2.2918	2.2918
p [deg/s]	-13.2171	**-10.8501**	-11.6662
q [deg/s]	**136.9195**	174.1044	183.2829
r [deg/s]	11.0615	**-8.5397**	-8.6573
	Overshoot (fault 2)		
	Proposed	BS	BS (tuned)
e_{1x} [m]	-0.0463	**0.0120**	0.0783
e_{1y} [m]	**0.0622**	-0.1038	0.1103
e_{1z} [m]	**0.0359**	0.1525	0.0775
$e_{1\phi}$ [deg]	**13.5692**	14.4542	14.9398
$e_{1\theta}$ [deg]	-7.5145	**0.3210**	0.7663
$e_{1\psi}$ [deg]	-0.9989	**-0.5990**	**-0.5990**
p [deg/s]	-80.2664	**-70.7518**	-74.2080
q [deg/s]	44.0333	**-2.0740**	-3.3816
r [deg/s]	-6.7852	**-3.9188**	-4.0077

The comparisons of standard deviation (STD) of the tracking error of position and Euler angle are summarized in Table 5.2. The comparison of the largest fluctuation after the fault in the position tracking error, Euler angle tracking error, and angular rate are summarized in Table 5.3. As shown in Table 5.2, the proposed controller can achieve the best robust position tracking performance among the considered controllers, although the STD of the tracking performance of Euler angle is higher than BS, due to the oscillation. As seen in Table 5.3, only the proposed controller maintains all the prescribed system constraints under actuator faults. More specially, the first fault affects the pitch angle/rate of the quadrotor, and the second fault affects the roll angle/rate of the quadrotor. After the first fault (see Overshoot (fault 1)), the fluctuation level of the pitch angle and rate has the smallest value in the proposed controller. Also, after the second fault (see Overshoot (fault 2)), the fluctuation level of the roll angle has the smallest value, even though the fluctuation level of the roll rate is the highest in the proposed controller. Finally, it can be stated that the proposed controller keeps the system states to maintain the prescribed bounds.

5.2 Case 2: Multiple Faults under Disturbances and Model Uncertainties.

To demonstrate the effectiveness of the proposed FTC scheme, multiple faults are considered for the system with disturbances and model uncertainties. The disturbances are chosen as [38, 39]:

$$\begin{aligned}\mathbf{d_p} &= \begin{bmatrix} 0.1\sin(t) - 0.2 + \dot{x}\dot{y} \\ 0.2\sin(\pi t) + \dot{y}\dot{z} \\ 0.2\sin(3t) - 0.1\sin(0.5\pi t) + e^{-t}\sin(t + \frac{\pi}{4}) \end{bmatrix} \\ \mathbf{d_r} &= \begin{bmatrix} -0.2\sin(0.5\pi t) + 0.1 \\ 0.1\cos(\sqrt{2}t) \\ 0.1\cos(2t+1) + 0.05 \end{bmatrix}\end{aligned} \tag{5.1}$$

Suppose that the output of position tracking controller e_{1i} for $i = x, y, z$ and the output of attitude controller r_{1j} for $j = \phi, \theta, \psi$ are contaminated by the noise $0.001\mathcal{N}(t)$, where $\mathcal{N}(t)$ is the standard Gaussian noise. The reference trajectory is constructed as:

$$\mathbf{p_d} = \left[\sin(\frac{t}{2})\cos(\frac{\pi t}{5})\cos(\frac{\pi}{4}),\ \sin(\frac{t}{2})\sin(\frac{\pi t}{5})\cos(\frac{\pi}{4}),\ -t\right]^T \tag{5.2}$$

The scenario of actuator efficiency losses is shown in Fig. 5.6.

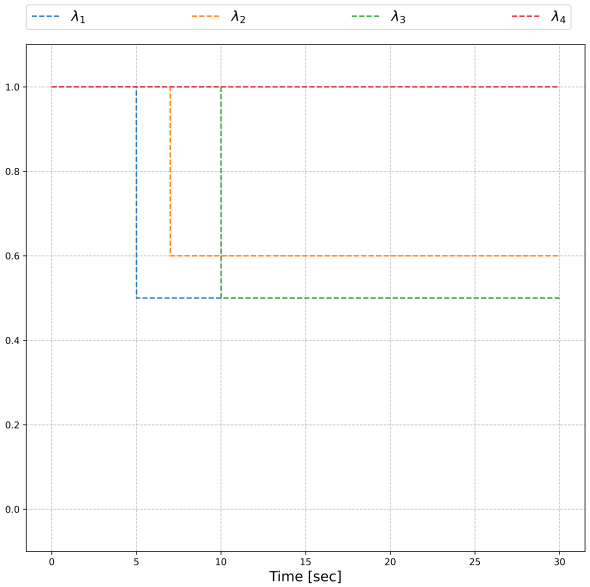

Figure 5.6: Actuator fault scenario (Actuator efficiency loss history: Case 2)

5.2.1 Case 2A

In this scenario, model uncertainties are considered as:

$$\begin{aligned} &\triangle m,\ \triangle I_{xx},\ \triangle I_{yy},\ \triangle I_{zz} = 0.1 \\ &\triangle c_f = 0.1, \quad \triangle c_\tau = -0.1 \end{aligned} \tag{5.3}$$

The parameter of the proposed controller are selected as $k_{1i} = 2$, $k_{2i} = 0.8$, and $k_{3i} = 0.5$, for $i = x, y, z$, and $k_{1i} = 15$, $k_{2i} = 50$, and $k_{3i} = 0.5$, for $j = \phi, \theta, \psi$. The predefined bounds for position errors are selected as $\rho_{0i} = 0.5$, $\rho_{\infty i} = 0.25$, and $\rho_{k_i} = 0.6$, for $i = x, y, z$, so that the position error cannot exceed 0.25m even if actuator fault occurs. For Euler angles and angular rates, $\rho_{1i} = 45$ deg and $\rho_{2i} = 150$ deg/s, for $j = \phi, \theta$, and $\rho_{1i} = 45$ deg and $\rho_{2i} = 180$ deg/s, for $j = \psi$. For the auxiliary system in Eq. (3.10), $[c_{1i}, c_{2i}] = [20, 20]$. The parameter of ESOs are selected as $a_i = [3, 3, 1]$, for $i = x, y, z$ and $j = \phi, \theta, \psi$, $\theta' = 0.7$ for all ESOs, $[l_x, l_y, l_z] = [31, 31, 46]$, and $[l_\phi, l_\theta, l_\psi] = [153, 194, 55]$.

Simulation results are shown in Figs. 5.7-5.14. Figures 5.7-5.9 show the position tracking error, Euler angle, and angular rate, respectively. The different levels of fluctuations are shown due to the rapid changes of actuator effectiveness. Meanwhile, it can be shown that the proposed controller can maintain the system states within the prescribed bounds under actuator faults. Figure 5.10 shows the rotor command and the true rotor input. The control input signals are displayed in Fig. 5.11. The fluctuations occur at 5, 7, 10, 14, and 15 s, similar to the system states. The actual total disturbance values and their estimated value for both no-fault and fault cases are shown in Fig. 5.12. The estimates of total disturbances follow the time-varying actual values well, and the disturbances due to the faults are well estimated, even though some peaks exist when the faults occur. The change of actuator efficiency

affects disturbance estimation, leading to the peaking phenomenon of ESO, the control inputs, and consequently, the state variables.

The actual gain of the proposed controller and the approximated PID-like gain of position tracking controller and attitude controller are shown in Fig. 5.13 and Fig. 5.14, respectively. In Fig. 5.13, the actual gain value approaches the PID-like gain value as time increases, as discussed in Chapter 4.2.1 and Remark 4.3. Also, as shown in Fig. 5.14, the actual gain value is similar to the PID-like gain value except i) at the beginning of the control and ii) when the actuator fault occurs, as discussed in Chapter 4.2.2 and Remark 4.6.

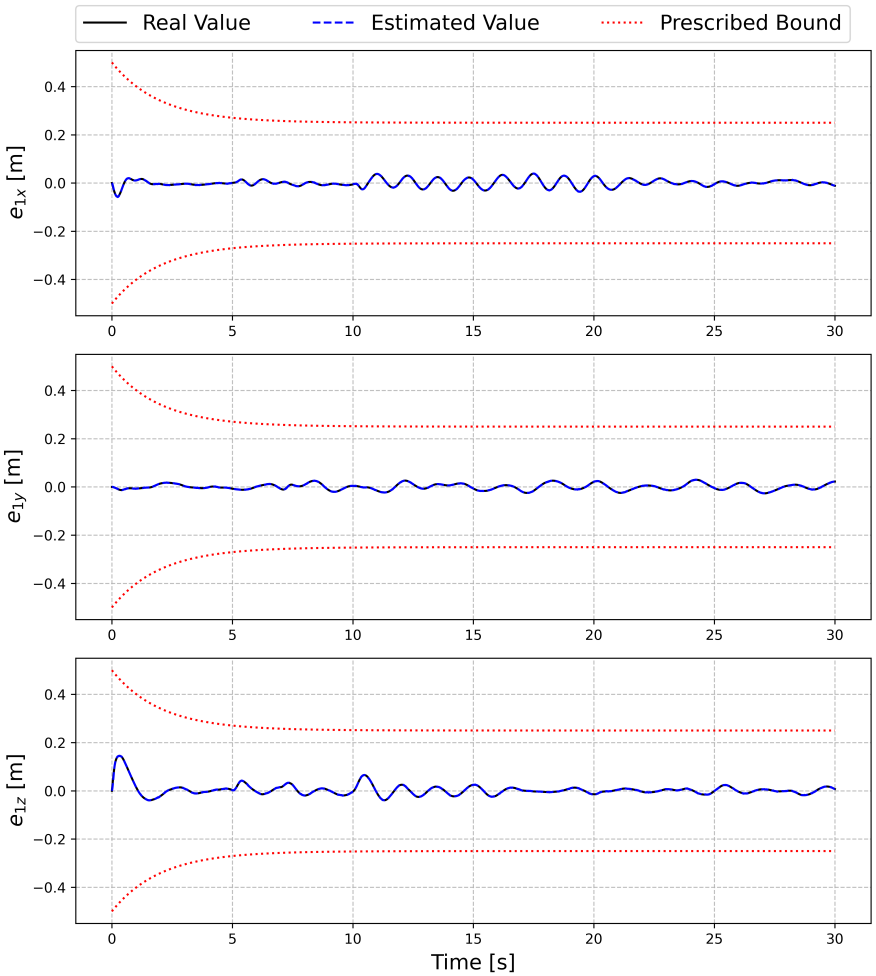

Figure 5.7: Position tracking errors and estimation responses (Case 2A)

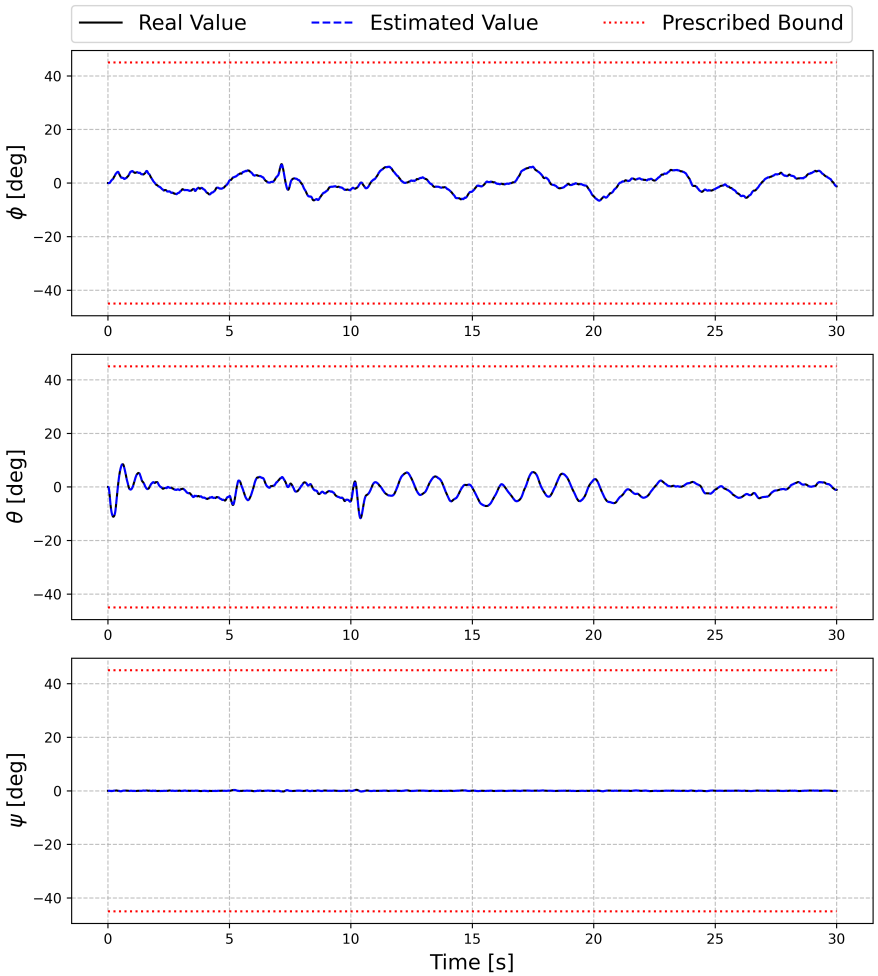

Figure 5.8: Euler angles, desired Euler angles, and estimation responses (Case 2A)

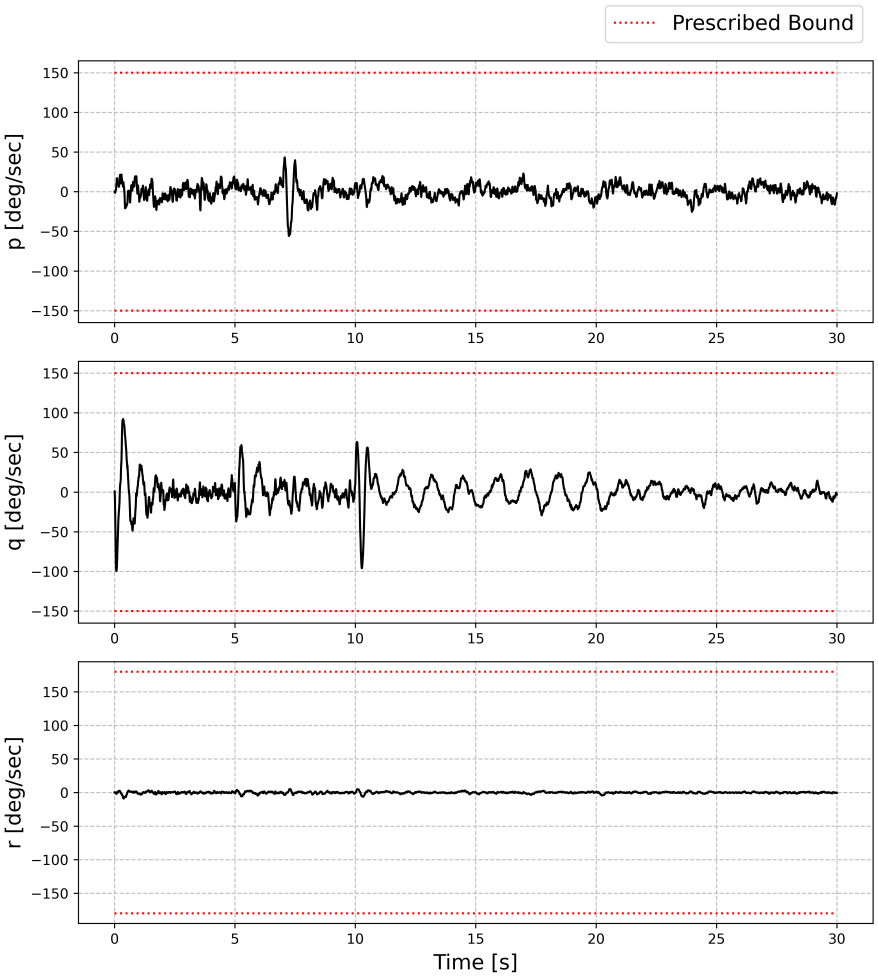

Figure 5.9: Angular rate responses (Case 2A)

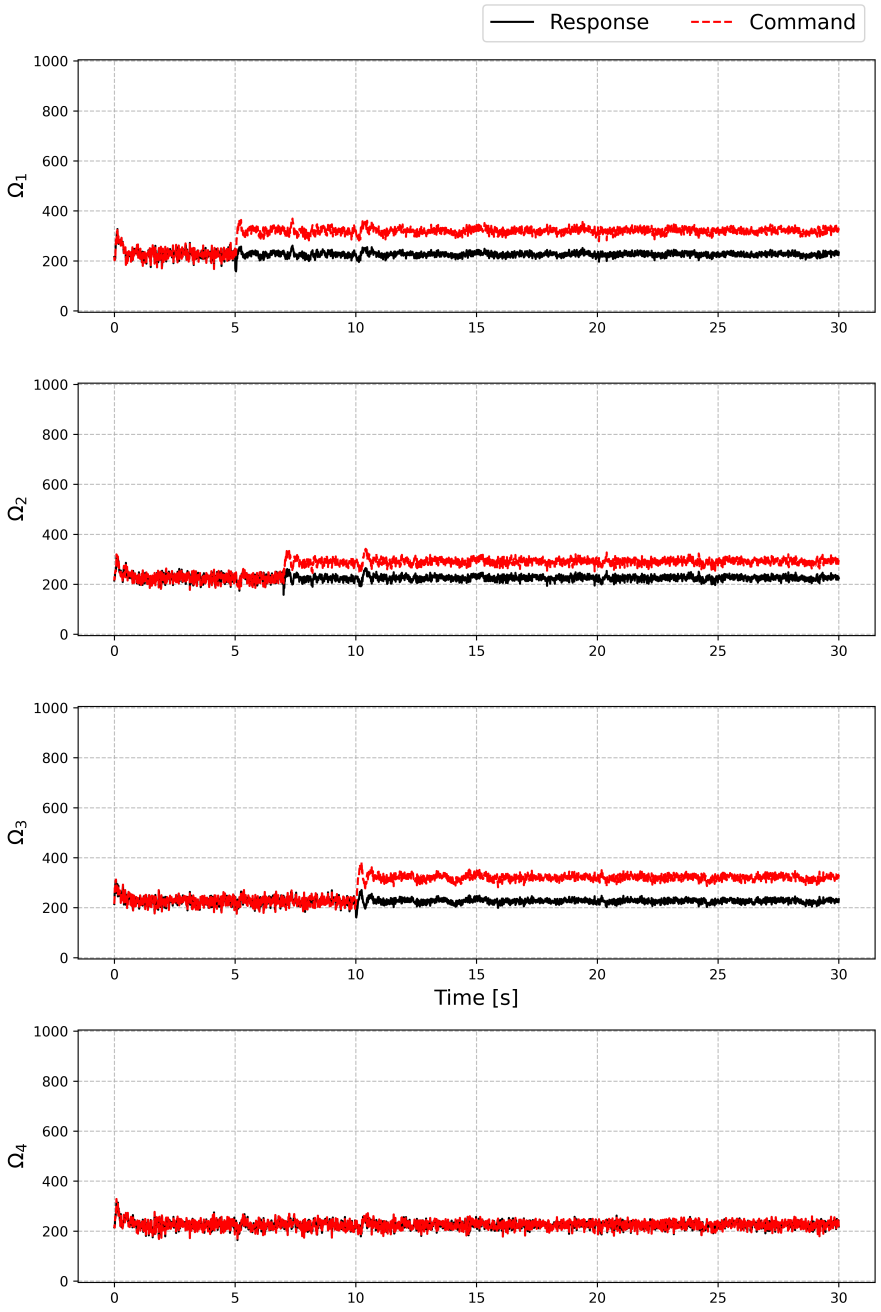

Figure 5.10: Rotor input responses (Case 2A)

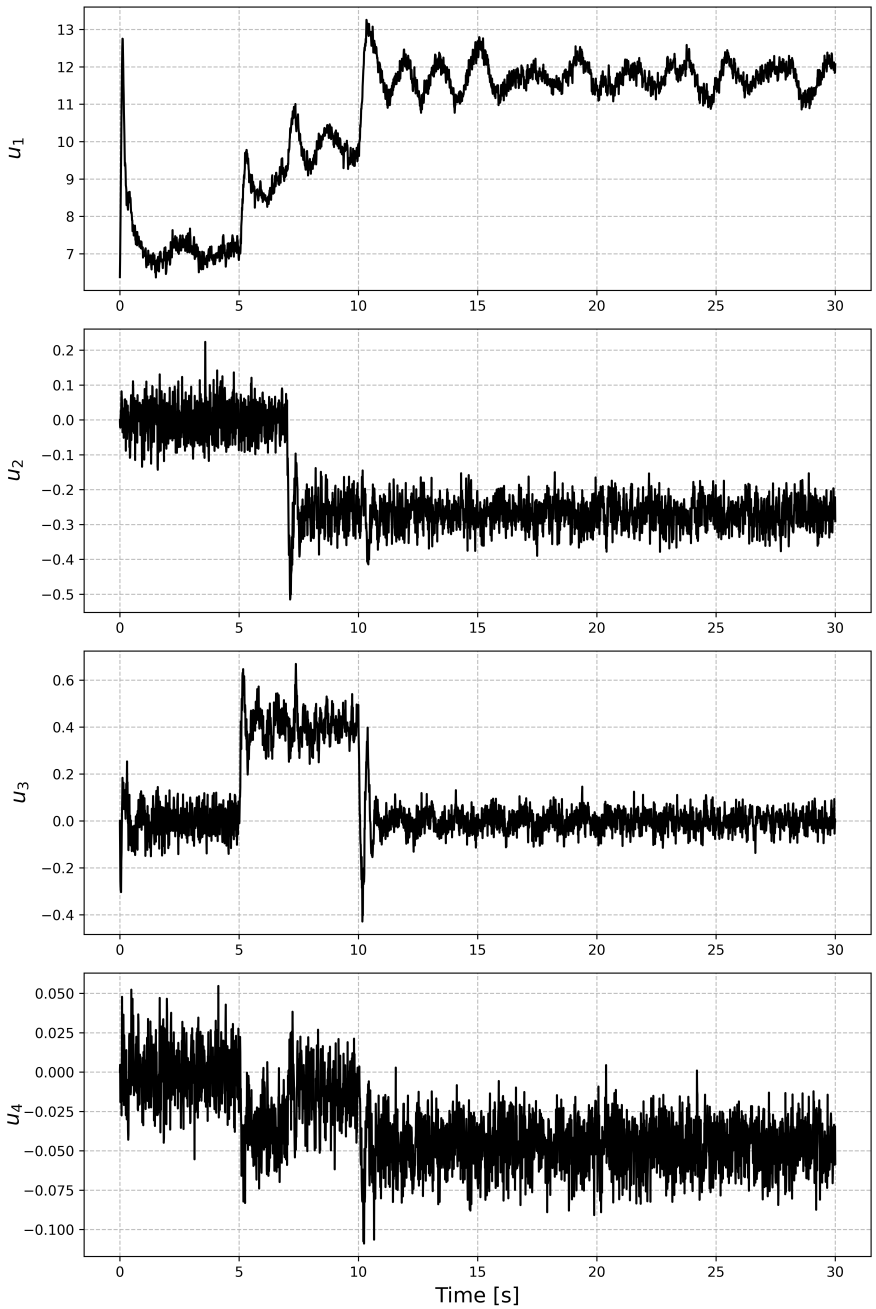

Figure 5.11: Control input responses (Case 2A)

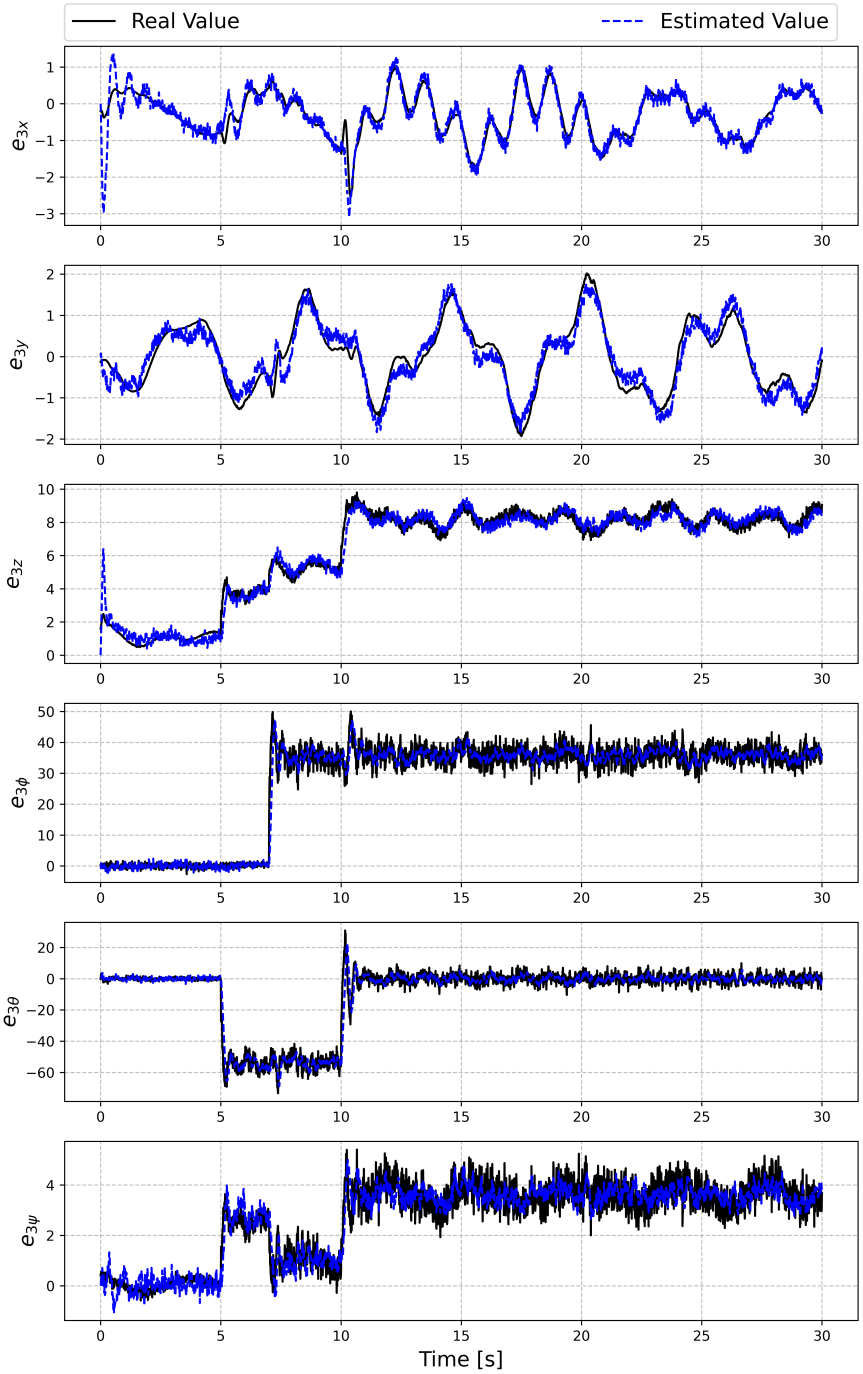

Figure 5.12: Real and estimated value of total disturbances (Case 2A)

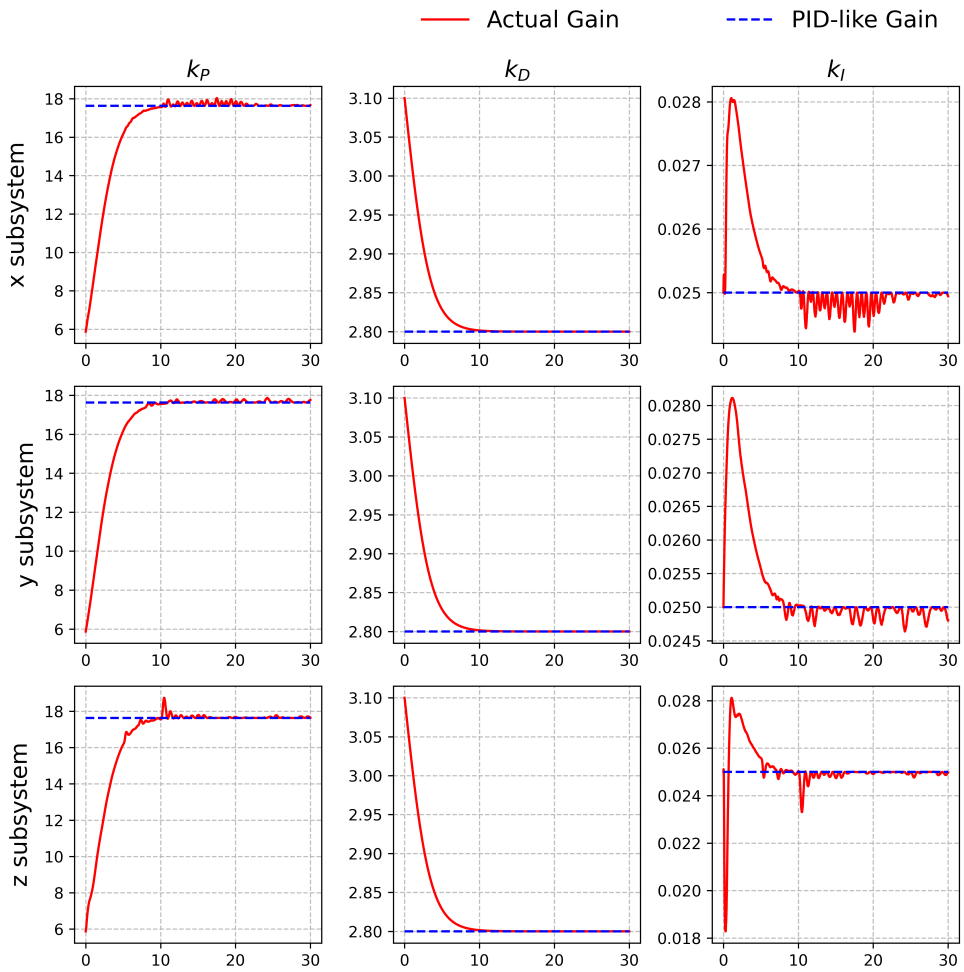

Figure 5.13: Real and PID-like gain of position controller (Case 2A)

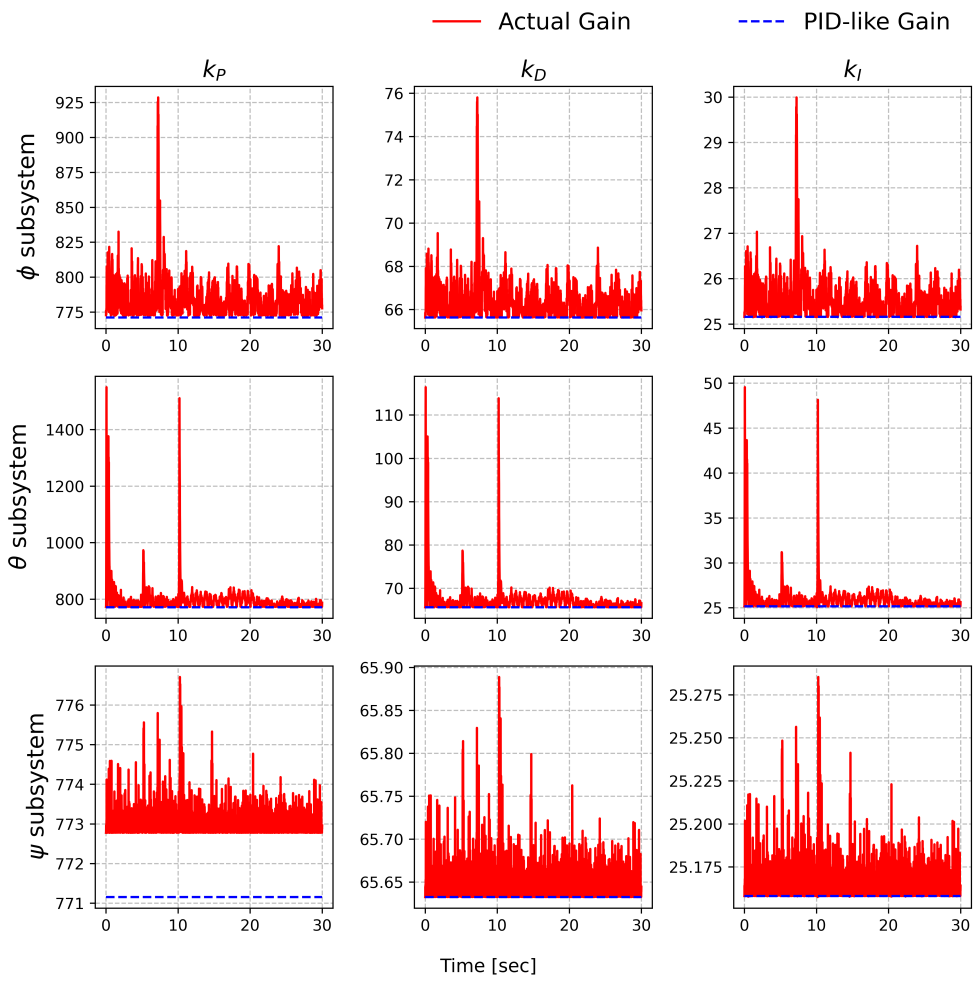

Figure 5.14: Real and PID-like gain of attitude controller (Case 2A)

5.2.2 Case 2B

In this scenario, the model uncertainties are considered as:

$$\begin{aligned} &\triangle m,\ \triangle I_{xx},\ \triangle I_{yy},\ \triangle I_{zz} = -0.1 \\ &\triangle c_f = 0.1, \quad \triangle c_\tau = -0.1 \end{aligned} \tag{5.4}$$

The parameter of the proposed controller are selected as $k_{1i} = 2$, $k_{2i} = 0.8$, and $k_{3i} = 0.5$, for $i = x, y, z$, and $k_{1i} = 15$, $k_{2i} = 50$, and $k_{3i} = 0.5$, for $j = \phi, \theta, \psi$. The predefined bounds for position errors are selected as $\rho_{0i} = 0.5$, $\rho_{\infty i} = 0.25$, and $\rho_{k_i} = 0.6$, for $i = x, y, z$, so that the position error cannot exceed 0.25m even if actuator fault occurs. For Euler angles and angular rates, $\rho_{1i} = 45$ deg and $\rho_{2i} = 150$ deg/s, for $j = \phi, \theta$, and $\rho_{1i} = 45$ deg and $\rho_{2i} = 180$ deg/s, for $j = \psi$. For the auxiliary system in Eq. (3.10), $[c_{1i}, c_{2i}] = [20, 20]$. The parameter of ESOs are selected as $a_i = [3, 3, 1]$, for $i = x, y, z$ and $j = \phi, \theta, \psi$, $\theta' = 0.7$ for all ESOs, $[l_x, l_y, l_z] = [30, 30, 40]$, and $[l_\phi, l_\theta, l_\psi] = [153, 194, 55]$.

Simulation results are shown in Figs. 5.15-5.22. The overall results are similar as in Case 2A. Figures 5.15-5.17 show the position tracking error, Euler angle, and angular rate, respectively. The different levels of fluctuations are shown due to the rapid changes of actuator effectiveness. Meanwhile, it can be shown that the proposed controller can maintain the system states within the prescribed bounds under actuator faults. Figure 5.18 shows the rotor command and the true rotor input. The control input signals are displayed in Fig. 5.19. The fluctuations occur at 5, 7, 10, 14, and 15 s, similar to the system states. The actual total disturbance values and their estimated value for both no-fault and fault cases are shown in Fig. 5.20. The estimates of total disturbances follow the time-varying actual values well, and the disturbances due to the faults are well estimated, even though some peaks exist when the faults occur. The

change of actuator efficiency affects disturbance estimation, leading to the peaking phenomenon of ESO, the control inputs, and consequently, the state variables.

The actual gain of the proposed controller and the approximated PID-like gain of position tracking controller and attitude controller are shown in Fig. 5.21 and Fig. 5.22, respectively. In Fig. 5.21, the actual gain value approaches the PID-like gain value as time increases, as discussed in Chapter 4.2.1 and Remark 4.3. Also, as shown in Fig. 5.22, the actual gain value is similar to the PID-like gain value except i) at the beginning of the control and ii) when the actuator fault occurs, as discussed in Chapter 4.2.2 and Remark 4.6.

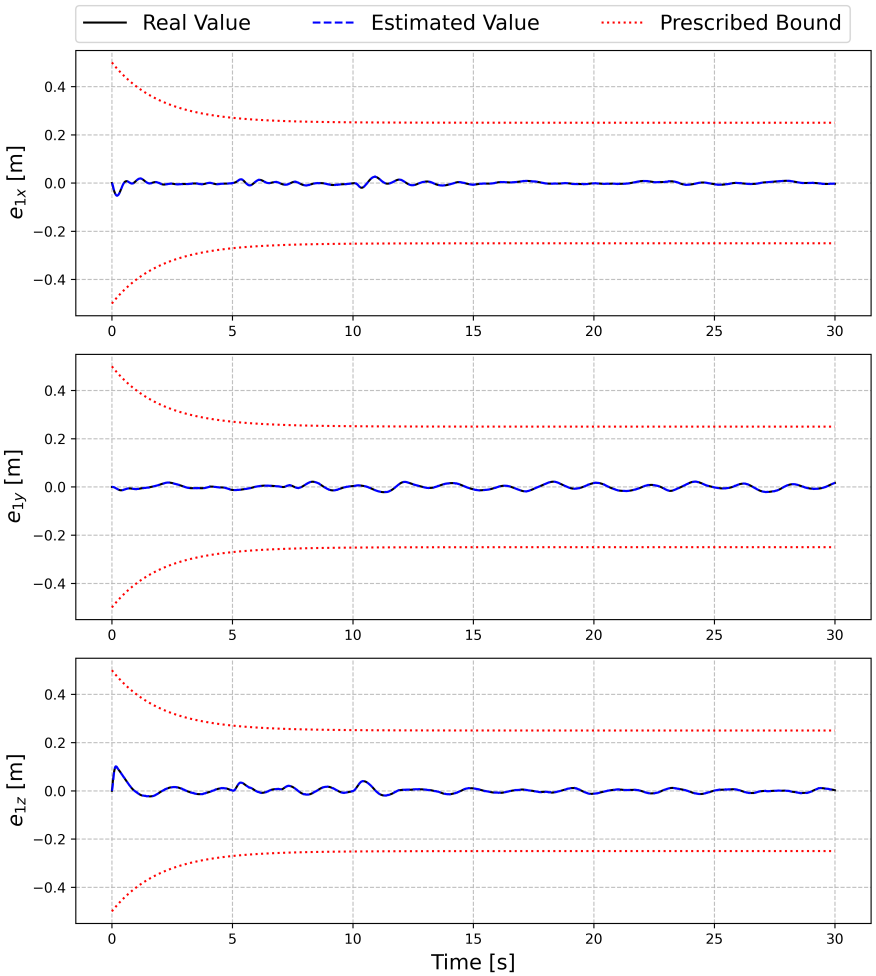

Figure 5.15: Position tracking errors and estimation responses (Case 2B)

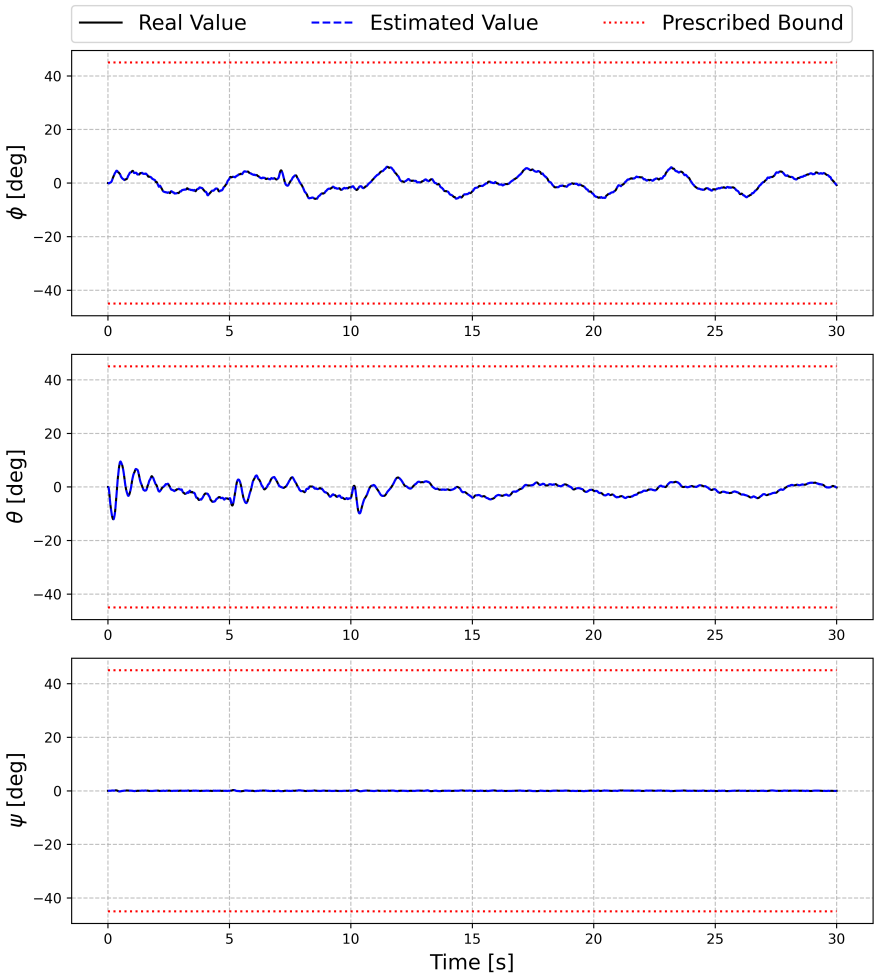

Figure 5.16: Euler angles, desired Euler angles, and estimation responses (Case 2B)

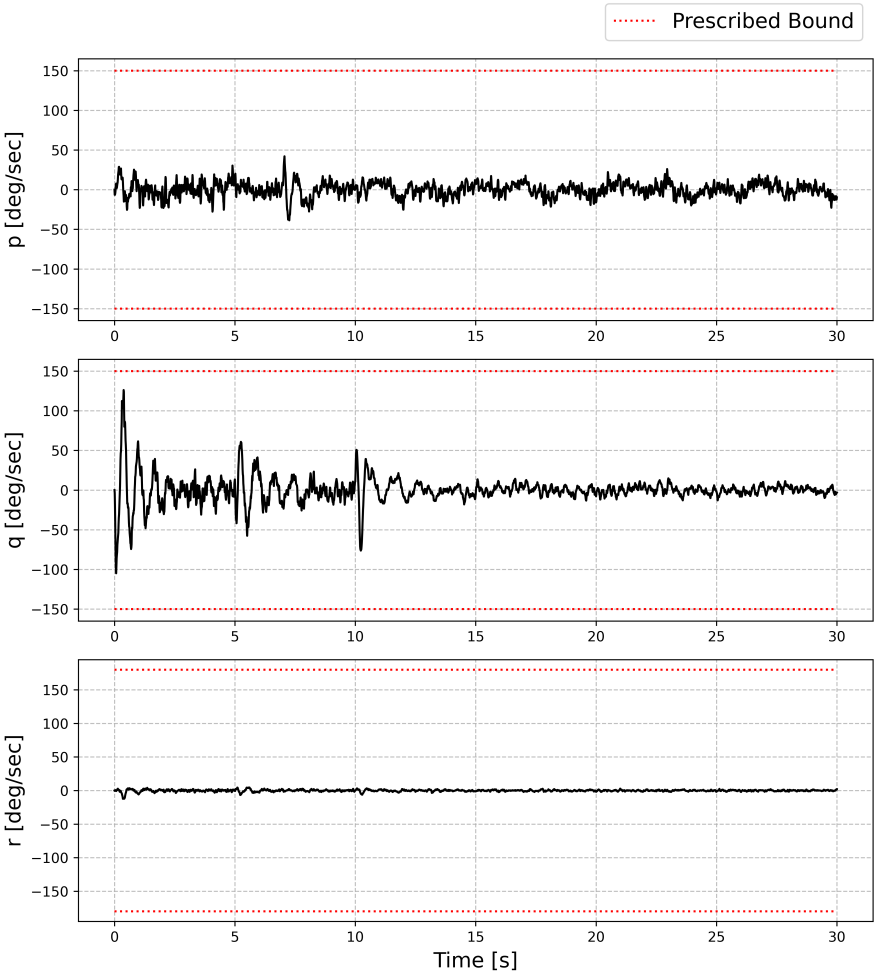

Figure 5.17: Angular rate responses (Case 2B)

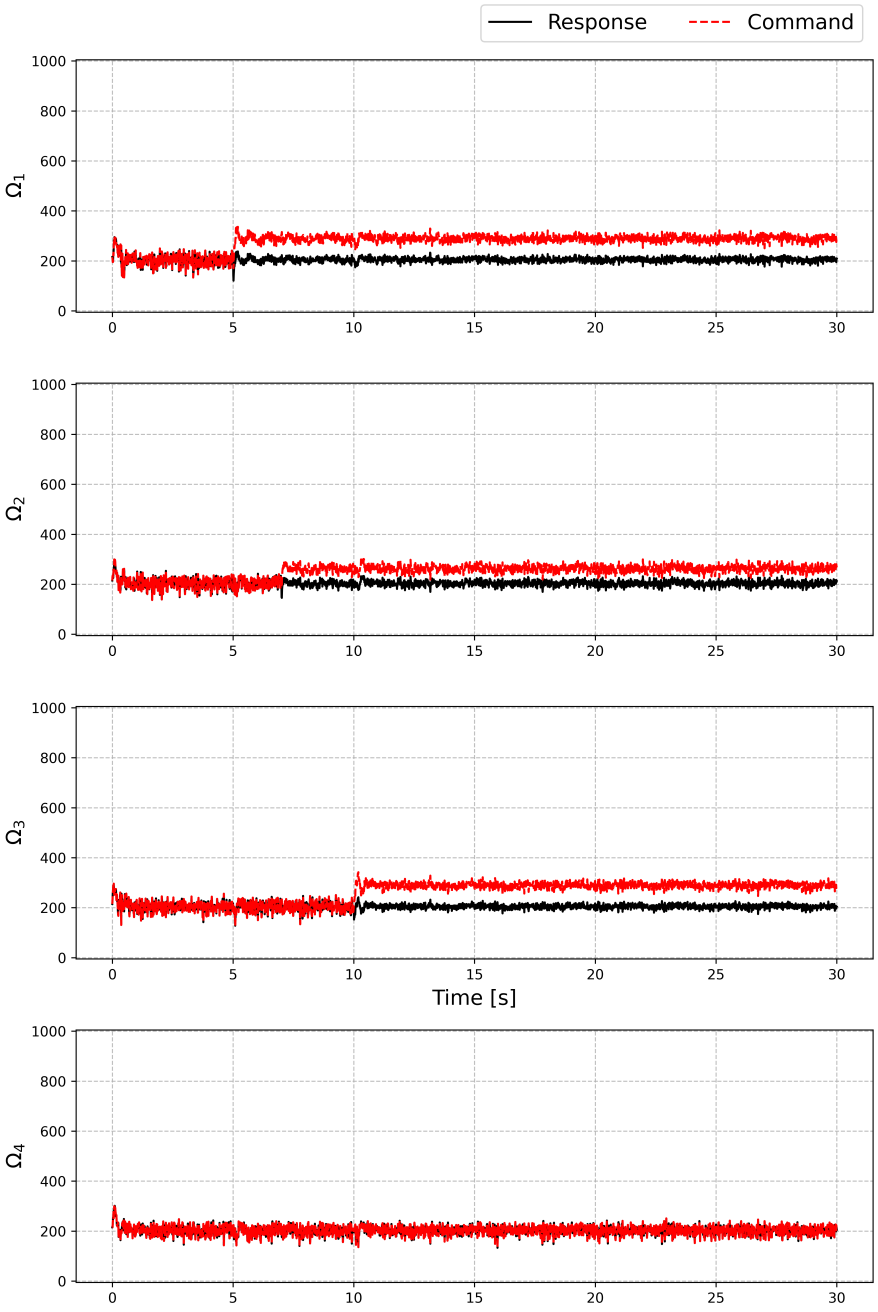

Figure 5.18: Rotor input responses (Case 2B)

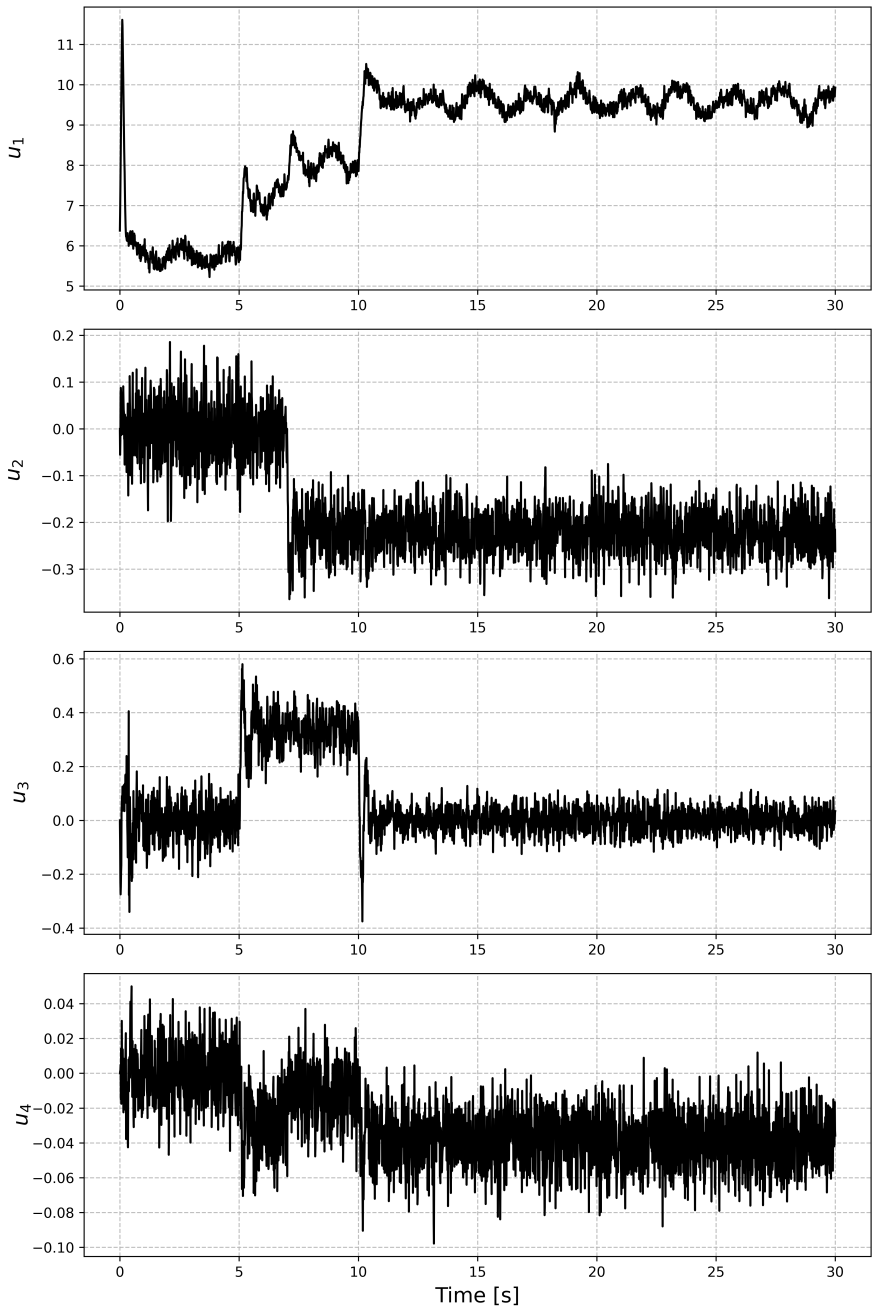

Figure 5.19: Control input responses (Case 2B)

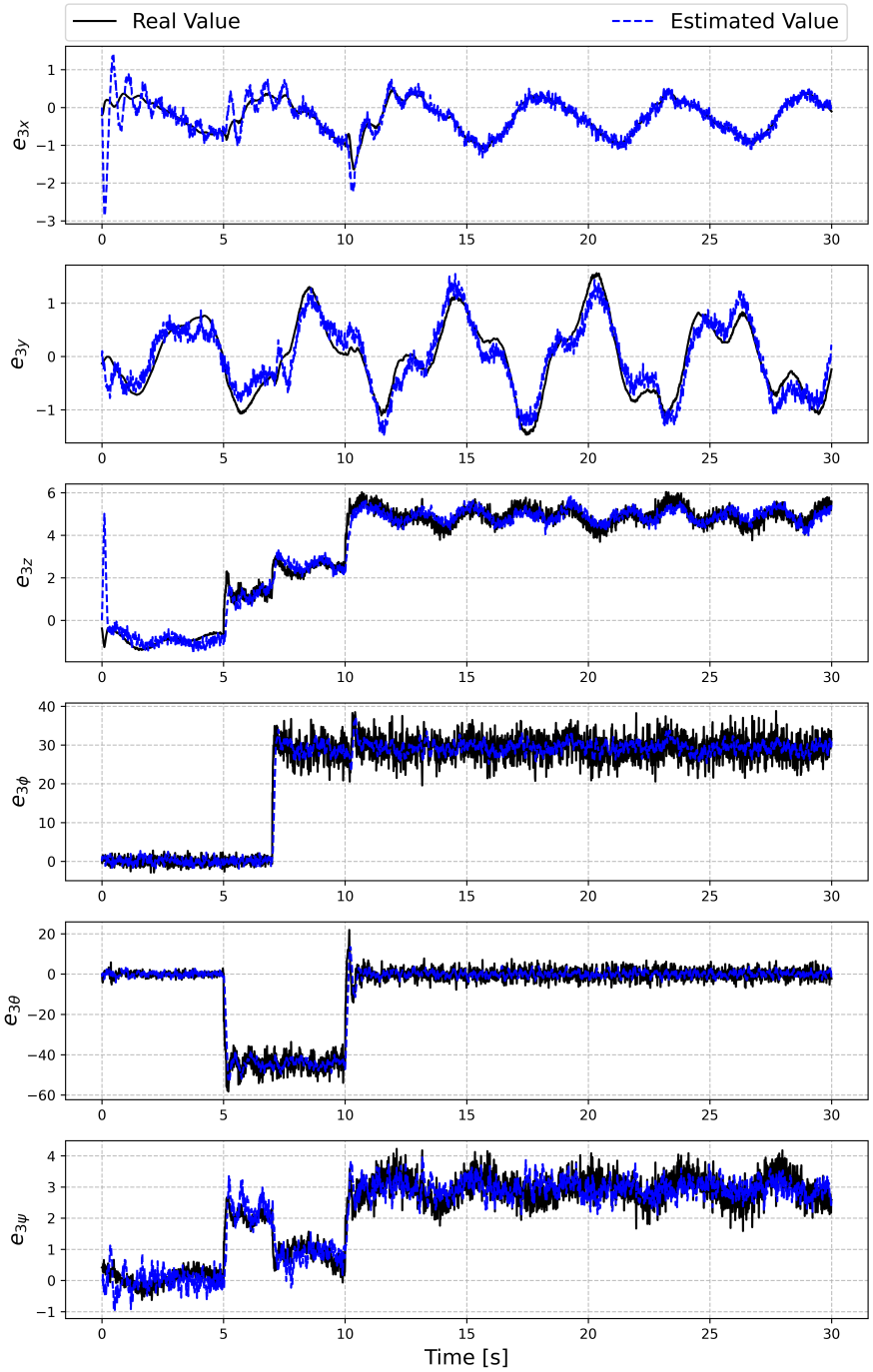

Figure 5.20: Real and estimated value of total disturbances (Case 2B)

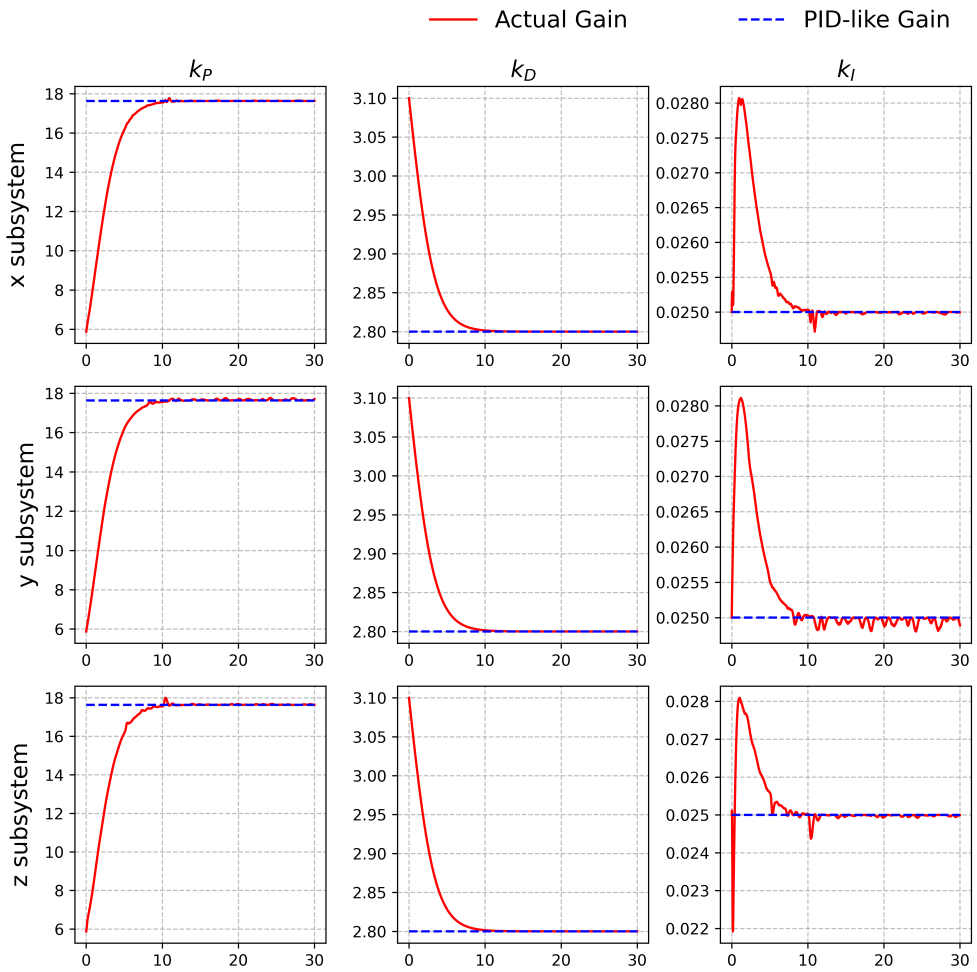

Figure 5.21: Real and PID-like gain of position controller (Case 2B)

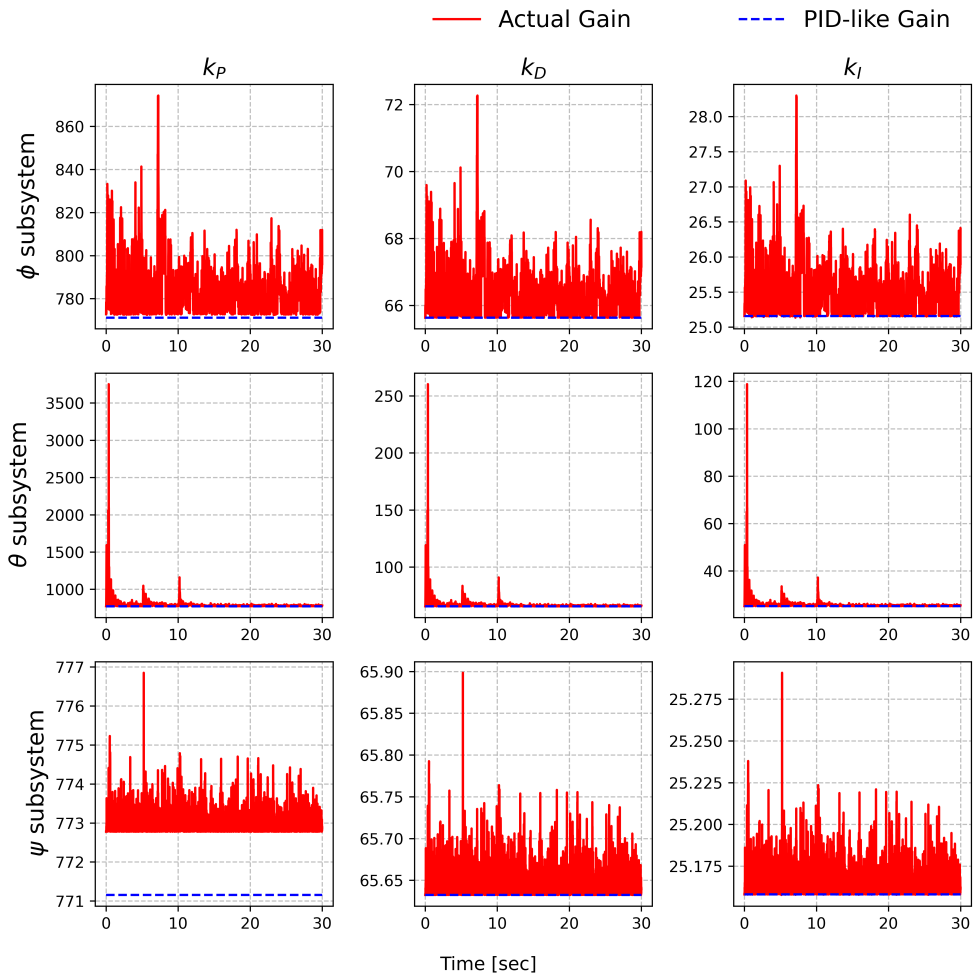

Figure 5.22: Real and PID-like gain of attitude controller (Case 2B)

Chapter 6

Conclusions

Fault tolerant control method based on barrier Lyapunov function and nonlinear extended state observer was proposed for a system subject to state constraints, disturbances, and model uncertainties. The system considered in this study is the quadrotor under actuator fault. Nonlinear extended state observer estimates the system states and total disturbances to compensate the effects of uncertainties and faults. Barrier Lyapunov function-based controllers was designed for guaranteeing the boundness of the position tracking errors, Euler angles, and angular rates. Furthermore, the analogy between the proposed control law and proportional-integral-derivative (PID) control law is analyzed. The relationship between the proposed control gains and PID control gains were shown in the form of a third-order polynomial. The effects of nonlinear estimator gains on the system responses were also proposed. Numerical simulations demonstrated that the proposed control method can achieve prescribed tracking performance and transient performance under disturbances and faults.

Reducing the peaking phenomenon of the extended state observer when fault occurs and real implementation remain as the future work.

Bibliography

[1] Luukkonen, T., "Modelling and control of quadcopter," *Independent Research Project in Applied Mathematics*, *Espoo*, Aalto University, 2011, pp. 22.

[2] Tayebi, A. and McGilvray, S., "Attitude stabilization of a VTOL quadrotor aircraft," *IEEE Transactions on Control Systems Technology*, Vol. 14, No. 3, 2006, pp. 562–571.

[3] Li, X., Zhang, H., Fan, W., Wang, C., and Ma, P., "Finite-time control for quadrotor based on composite barrier Lyapunov function with system state constraints and actuator faults," *Aerospace Science and Technology*, Vol. 119, 2021, pp. 107063.

[4] Kim, Y. and Kim, S., *Reconfigurable flight control*, Vol. 5 of *Dynamics and Control*, Part 23: Flight Control, Encyclopedia of Aerospace Engineering, Wiley, 2010.

[5] Falconí, G. P. and Holzapfel, F., "Adaptive fault tolerant control allocation for a hexacopter system," *2016 American Control Conference (ACC)*, Boston, MA, July, 2016.

[6] Alwi, H. and Edwards, C., "Fault tolerant control using sliding modes with online control allocation," *Automatica*, Vol. 44, No. 7, 2008, pp. 1859– 1866.

[7] Wang, B. and Zhang, Y., "An adaptive fault-tolerant sliding mode control allocation scheme for multirotor helicopter subject to simultaneous actuator faults," *IEEE Transactions on Industrial Electronics*, Vol. 65, No. 5, 2017, pp. 4227–4236.

[8] Aboudonia, A., El-Badawy, A., and Rashad, R., "Disturbance observer-based feedback linearization control of an unmanned quadrotor helicopter," *Proceedings of the Institution of Mechanical Engineers, Part I: Journal of Systems and Control Engineering*, Vol. 230, No. 9, 2016, pp. 877–891.

[9] Chamseddine, A., Zhang, Y., Rabbath, C.-A., Apkarian, J., and Fulford, C., "Model reference adaptive fault tolerant control of a quadrotor UAV," Infotech@ Aerospace conference, St. Louis, MO, Mar. 2011.

[10] Han, J., "From PID to active disturbance rejection control," *IEEE Transactions on Industrial Electronics*, Vol. 56, No. 3, 2009, pp. 900–906.

[11] Shao, X., Liu, J., Cao, H., Shen, C., and Wang, H., "Robust dynamic surface trajectory tracking control for a quadrotor UAV via extended state observer," *International Journal of Robust and Nonlinear Control*, Vol. 28, No. 7, 2018, pp. 2700–2719.

[12] Zhao, L., Dai, L., Xia, Y., and Li, P., "Attitude control for quadrotors subjected to wind disturbances via active disturbance rejection control and integral sliding mode control," *Mechanical Systems and Signal Processing*, Vol. 129, No. 4, 2019, pp. 531–545.

[13] Astolfi, D., Marconi, L., and Teel, A., "Low-power peaking-free high-gain observers for nonlinear systems," *2016 European Control Conference (ECC)*, IEEE, Aalborg, Denmark, Jun. 2016.

[14] Astolfi, D., Marconi, L., Praly, L., and Teel, A. R., "Low-power peaking-free high-gain observers," *Automatica*, Vol. 98, No. 4, 2018, pp. 169–179.

[15] Zhao, Z.-L., Ma, P., and Chen, S., "A new nonlinear extended state observer design for output tracking of uncertain nonlinear systems," *Advanced Control for Applications: Engineering and Industrial Systems*, Vol. 3, No. 2, 2021, pp. e46.

[16] Zhao, Z.-L. and Guo, B.-Z., "A novel extended state observer for output tracking of MIMO systems with mismatched uncertainty," *IEEE Transactions on Automatic Control*, Vol. 63, No. 1, 2017, pp. 211–218.

[17] Zhao, Z.-L. and Guo, B.-Z., "A nonlinear extended state observer based on fractional power functions," *Automatica*, Vol. 81, 2017, pp. 286–296.

[18] Derafa, L., Madani, T., and Benallegue, A., "Dynamic modeling and experimental identification of four rotors helicopter parameters," *IEEE International Conference on Industrial Technology*, Mumbai, India, Dec, 2006.

[19] Dai, S.-L., He, S., Wang, M., and Yuan, C., "Adaptive neural control of underactuated surface vessels with prescribed performance guarantees," *IEEE Transactions on Neural Networks and Learning Systems*, Vol. 30, No. 12, 2018, pp. 3686–3698.

[20] Ngo, K. B., Mahony, R., and Jiang, Z.-P., "Integrator backstepping using barrier functions for systems with multiple state constraints," *Proceedings of the 44th IEEE Conference on Decision and Control*, Seville, Spain, Dec. 2005.

[21] Tee, K. P., Ge, S. S., and Tay, E. H., "Barrier Lyapunov functions for the control of output-constrained nonlinear systems," *Automatica*, Vol. 45, No. 4, 2009, pp. 918–927.

[22] Tee, K. P. and Ge, S. S., "Control of nonlinear systems with partial state constraints using a barrier Lyapunov function," *International Journal of Control*, Vol. 84, No. 12, 2011, pp. 2008–2023.

[23] Tee, K. P., Ren, B., and Ge, S. S., "Control of nonlinear systems with time-varying output constraints," *Automatica*, Vol. 47, No. 11, 2011, pp. 2511– 2516.

[24] Kourani, A. and Daher, N., "A practical guideline for designing and tuning adaptive backstepping controllers for a class of second-order systems based on PID similarity," *International Journal of Dynamics and Control*, Vol. 10, No. 2, 2022, pp. 1829-1846.

[25] Yu, J., Shi, P., and Zhao, L., "Finite-time command filtered backstepping control for a class of nonlinear systems," *Automatica*, Vol. 92, No. 3, 2018, pp. 173–180.

[26] Kartal, Y., Kolaric, P., Lopez, V., Dogan, A., and Lewis, F., "Backstepping approach for design of PID controller with guaranteed performance for micro-air UAV," *Control Theory and Technology*, Vol. 18, No. 1, 2020, pp. 19–33.

[27] Skjetne, R. and Fossen, T. I., "On integral control in backstepping: Analysis of different techniques," 2004 *American Control Conference (ACC)*, Boston, MA, Jun. 30-Jul-2, 2004.

[28] Nohooji, H. R., "Constrained neural adaptive PID control for robot manipulators," *Journal of the Franklin Institute*, Vol. 357, No. 7, 2020, pp. 3907– 3923.

[29] Sontag, E. D., *Mathematical control theory: deterministic finite dimensional systems*, Vol. 6, Springer Science Business Media, Berlin/Heidelberg, Germany, 2013.

[30] Ren, B., Ge, S. S., Tee, K. P., and Lee, T. H., "Adaptive neural control for output feedback nonlinear systems using a barrier Lyapunov function," *IEEE Transactions on Neural Networks*, Vol. 21, No. 8, 2010, pp. 1339– 1345.

[31] Sun, Y., Dong, D., Qin, H., and Wang, W., "Distributed tracking control for multiple Euler–Lagrange systems with communication delays and input saturation," *ISA Transactions*, Vol. 96, 2020, pp. 245–254.

[32] Kim, M., Lee, H., Kim, J., Kim, S., and Kim, Y., "Hierarchical fault tolerant control of a hexacopter UAV against actuator failure," *International Conference on Robot Intelligence Technology and Applications(RiTA)*, Daejeon, Korea, Dec. 2021.

[33] Shi, D., Wu, Z., and Chou, W., "Generalized extended state observer based high precision attitude control of quadrotor vehicles subject to wind disturbance," *IEEE Access*, Vol. 6, 2018, pp. 32349–32359.

[34] Dydek, Z. T., Annaswamy, A. M., and Lavretsky, E., "Adaptive control of quadrotor UAVs: A design trade study with flight evaluations," *IEEE Transactions on Control Systems Technology*, Vol. 21, No. 4, 2012, pp. 1400–1406.

[35] Zhou, J. and Wen, C., "Robust adaptive control of uncertain nonlinear systems in the presence of input saturation," *IFAC Proceedings Volumes*, Vol. 39, No. 1, 2006, pp. 149–154.

[36] An, H., Liu, J., Wang, C., and Wu, L., "Disturbance observer-based anti-windup control for air-breathing hypersonic vehicles," *IEEE Transactions on Industrial Electronics*, Vol. 63, No. 5, 2016, pp. 3038–3049.

[37] Vepa, R., *Nonlinear control of robots and unmanned aerial vehicles: an integrated approach*, Crc Press, Boca Ration, FL, 2016.

[38] Jia, Z., Yu, J., Mei, Y., Chen, Y., Shen, Y., and Ai, X., "Integral backstepping sliding mode control for quadrotor helicopter under external uncertain disturbances," *Aerospace Science and Technology*, Vol. 68, 2017, pp. 299– 307.

[39] Li, X., Zhang, H., Fan, W., Zhao, J., and Wang, C., "Multivariable finite-time composite control strategy based on immersion and invariance for quadrotor under mismatched disturbances," *Aerospace Science and Technology*, Vol. 99, No. 2, Article 105763, 2020.

국문초록

본 논문에서는 배리어 르아프노프 함수와 비선형 확장상태 관측기를 사용하여 쿼드로터 시스템 구속조건, 외란, 모델 불확실성 하에서 구동기 고장이 발생하였을 때 대응하는 고장허용 제어기를 제안하였다. 본 논문에서 제안한 고장허용 제어기는 이중 루프 구성으로 위치 추종 제어기와 자세 제어기로 이루어져 있다. 시불변계 및 시변계 배리어 르야프노프 함수를 사용하여 정상상태 및 과도상태에서의 성능이 보장되며, 비선형 확장상태 관측기의 사용으로 외란, 모델 불확실성, 그리고 구동기 고장에 의한 영향을 보상하였다. 또한, 비례-적분-미분 제어기와의 유사성과 비선형 확장상태 관측기에 의한 영향을 고려하여, 제안하는 제어기의 제어이득을 튜닝하기 위한 실용적인 가이드라인을 제시하였다. 제어기의 성능을 확인하기 위해 다양한 시나리오에 대해 수치 시뮬레이션을 수행하였다.

주요어: 구동기 고장, 배리어 르아프노프 함수, 고장허용제어, 비선형 확장상태 관측기
학번: 2021-27861